# Validation of GEMS tropospheric $NO_2$ columns and their diurnal variation with ground-based DOAS measurements

Kezia Lange[1], Andreas Richter[1], Tim Bösch[1], Bianca Zilker[1], Miriam Latsch[1], Lisa K. Behrens[1], Chisom M. Okafor[1], Hartmut Bösch[1], John P. Burrows[1], Alexis Merlaud[2], Gaia Pinardi[2], Caroline Fayt[2], Martina M. Friedrich[2], Ermioni Dimitropoulou[2], Michel Van Roozendael[2], Steffen Ziegler[3], Simona Ripperger-Lukosiunaite[3], Leon Kuhn[3], Bianca Lauster[3], Thomas Wagner[3], Hyunkee Hong[4], Donghee Kim[4], Lim-Seok Chang[4], Kangho Bae[5,6], Chang-Keun Song[5,6,7], Jong-Uk Park[8], and Hanlim Lee[9]

[1]Institute of Environmental Physics, University of Bremen, Bremen, Germany
[2]Royal Belgian Institute for Space Aeronomy, Brussels, Belgium
[3]Max Planck Institute for Chemistry, Mainz, Germany
[4]Environmental Satellite Center, National Institute of Environmental Research, Incheon, Republic of Korea
[5]Department of Civil, Urban, Earth and Environmental Engineering, Ulsan National Institute of Science and Technology, Ulsan, Republic of Korea
[6]Research & Management Center for Particulate Matters at the Southeast Region of Korea, Ulsan National Institute of Science and Technology, Ulsan, Republic of Korea
[7]School of Carbon Neutrality, Ulsan National Institute of Science and Technology, Ulsan, Republic of Korea
[8]School of Earth and Environmental Sciences, Seoul National University, Seoul, Republic of Korea
[9]Division of Earth Environmental System Science, Major of Spatial Information Engineering, Pukyong National University, Busan, Republic of Korea

**Correspondence:** Kezia Lange (klange@iup.physik.uni-bremen.de)

**Abstract.** Instruments for air quality observations on geostationary satellites provide multiple observations per day and allow for the analysis of the diurnal variation of important air pollutants such as nitrogen dioxide ($NO_2$). The South Korean instrument GEMS, launched in February 2020, is the first geostationary instrument that is able to observe the diurnal variation of $NO_2$. The measurements have a spatial resolution of $3.5\,\mathrm{km} \times 8\,\mathrm{km}$, and cover a large part of Asia.

This study compares one year of tropospheric $NO_2$ vertical column density (VCD) observations from the operational GEMS L2 product, the scientific GEMS IUP-UB product, the operational TROPOMI product, and ground-based DOAS measurements in South Korea. The GEMS L2 tropospheric $NO_2$ VCDs overestimate the ground-based tropospheric $NO_2$ VCDs with a median relative difference of +61 % and a correlation coefficient of 0.76. The median relative difference is -2 % for the GEMS IUP-UB product and -16 % for the TROPOMI product, with correlation coefficients of 0.83 and 0.89 respectively. The scatter in the GEMS products can be reduced when observations are limited to the TROPOMI overpass time.

Diurnal variations of tropospheric $NO_2$ VCDs differ by pollution level of the analyzed site but with good agreement between the GEMS IUP-UB and ground-based observations. Low polluted sites show weak or almost no diurnal variation. In summer, the polluted sites show a minimum around noon, indicating the large influence of photochemical loss. Most variation is seen in spring and autumn, with increasing $NO_2$ in the morning, a maximum close to noon, and a decrease towards the afternoon. Winter observations show rather flat or slightly decreasing $NO_2$ over the day. Winter observations under low wind conditions

at high polluted sites show enhancements of $NO_2$ over the day. This indicates that under calm conditions, dilution and the less effective chemical loss in winter do not balance the accumulating emissions. Diurnal variation observed at a low polluted site follows seasonal wind patterns.

Weekday-weekend effect analysis shows good agreement between the different products. However, the GEMS L2 product while agreeing with the other data sets during weekdays shows significantly less reduction on weekends.

The influence of the stratospheric contribution and the surface reflectivity product on the satellite tropospheric $NO_2$ VCD products are investigated. While the TM5 model's stratospheric VCDs, used in the TROPOMI product, are too high, resulting in too low and even negative tropospheric $NO_2$ VCDs, when used in the GEMS IUP-UB retrieval, the GEMS L2 stratospheric VCD is too low. Surface reflectivity comparisons indicate that the GEMS L2 reflectivity has a large contribution to the observed overestimation and scatter.

## 1 Introduction

Nitrogen oxides, in particular nitrogen monoxide (NO) and nitrogen dioxide ($NO_2$), collectively referred to as $NO_x$, are among the most important air pollutants and strongly impact tropospheric chemistry. $NO_x$ is emitted into the atmosphere by natural sources such as lightning and soil microbial processes, but the primary source is anthropogenic activities. Anthropogenic emissions result from fossil fuel combustion mainly for transportation, the industry and energy sectors, and residential heating (Seinfeld and Pandis, 2006; Wallace and Hobbs, 2006). High concentrations of $NO_x$ are a health hazard and of growing importance for environmental legislation, since most anthropogenic sources are concentrated in urban areas with high population densities (Faustini et al., 2014).

Tropospheric $NO_x$ is mainly emitted as NO, which is rapidly converted to $NO_2$ by the reaction with tropospheric ozone ($O_3$). Due to their short atmospheric lifetimes, on the order of a few hours in the boundary layer during daytime (Beirle et al., 2011), the heterogeneous distribution of sources and variations of meteorological conditions, tropospheric $NO_2$ shows high spatial and temporal variability. Monitoring and understanding this variability is necessary to better understand the contributions of emissions, tropospheric chemistry, and transport effects, especially in urban areas with large and heterogeneous $NO_x$ sources combined with high population densities.

To resolve this spatial and temporal variation of tropospheric $NO_2$, measurements with good spatial and temporal resolution are needed. $NO_2$ can be remotely observed using the DOAS (differential optical absorption spectroscopy) technique (Platt and Perner, 1980). DOAS measurements of $NO_2$ have been performed from different platforms, including ground-based stations, moving platforms such as cars, ships, or aircraft, and environmental satellites, with advantages and disadvantages regarding spatial and temporal resolution.

Stationary ground-based instruments such as multi axis DOAS (MAX-DOAS, see e.g., Hönninger et al. (2004); Wittrock et al. (2004); Herman et al. (2009)) provide several observations of $NO_2$ column densities per hour at a given location. These data sets are commonly continuous and are valuable for the validation of satellite data products, among other applications (e.g., Pinardi et al., 2020; Verhoelst et al., 2021).

Mobile car DOAS measurements enable the observation of the spatial distribution in addition to its temporal evolution and are an additional valuable source for the validation of satellite trace gas data products (e.g., Wagner et al., 2010). They fill a gap between stationary ground-based and satellite observations by mapping the variability within the satellite pixel and quantifying errors for satellite and stationary ground-based comparisons.

The advantage of measurements from environmental satellites in polar sun-synchronous low earth orbit (LEO) is that they can provide global coverage. The spatial resolution of satellite observations making use of the DOAS method has increased strongly since the first mission with a ground footprint of 320 km × 40 km for the Global Ozone Monitoring Experiment (GOME) in 1995 (Burrows et al., 1999) to the recent TROPOspheric Monitoring Instrument (TROPOMI) with a spatial resolution of 5.5 km × 3.5 km (Veefkind et al., 2012). TROPOMI measurements offers the possibility to deconvolve sources of $NO_x$, such as individual power plants, and to quantify their emissions (e.g., Beirle et al., 2019a). Satellite measurements also enable the seasonal variations of $NO_2$ to be observed globally. This has been done, for example, using SCIAMACHY (Bovensmann et al., 1999) observations to disentangle the sources of $NO_x$ (van der A et al., 2008) or using TROPOMI observations to analyze the seasonality of $NO_x$ emissions and lifetimes (Lorente et al., 2019; Lange et al., 2022).

Instruments in low earth orbits usually provide at best only one measurement per day and location in low and mid latitudes. Combining observations from several satellites with different overpass times provides some information about the diurnal variation of $NO_2$. Several studies have applied this method, based on the morning overpasses of the SCIAMACHY or GOME-2 (Munro et al., 2006) instrument and the early afternoon observation of the Ozone Monitoring Instrument (OMI, Levelt et al. (2006)), see e.g., Boersma et al. (2008, 2009); Penn and Holloway (2020). Boersma et al. (2008) used SCIAMACHY and OMI observations to estimate the diurnal variation of $NO_2$. Over urban regions, they found up to 40 % reduced $NO_2$ columns in the OMI afternoon overpass compared to the SCIAMACHY morning overpass. They explained this by photochemical loss, modulated by the diurnal cycle of anthropogenic emissions. Over biomass burning regions, they detected an increase from the morning to the afternoon overpass, which is consistent with fire counts from the geostationary satellites. Analyzing the differences between SCIAMACHY and OMI tropospheric $NO_2$ columns from Israeli cities, Boersma et al. (2009) found again 40 % reduction for $NO_2$ columns in the afternoon compared to the morning overpass during summer, and nearly no differences in winter with only slightly higher $NO_2$ in the afternoon. Penn and Holloway (2020) found around 1.5–2 times higher $NO_2$ columns for the morning compared to the afternoon overpass for large urban areas in the US using GOME-2 and OMI observations.

To analyze the diurnal variation of $NO_x$ in more detail, remote sensing instruments on satellites in geostationary orbit are essential (Burrows et al., 2004). The South Korean instrument GEMS (Geostationary Environmental Monitoring Spectrometer, Kim et al. (2020)) was launched in February 2020 and is the first instrument in geostationary orbit from which hourly daytime air quality data products, including $NO_2$, are retrieved. Positioned over the Equator at a longitude of 128.2°E, GEMS takes measurements with a spatial resolution of about $3.5\,\mathrm{km} \times 8\,\mathrm{km}$ over a large part of Asia. With up to 10 observations per day, GEMS data products offer a unique opportunity to investigate the diurnal variation of $NO_2$ and other trace gases. NASA's TEMPO (Zoogman et al., 2017) launched in April 2023 and ESA's Sentinel-4 (Ingmann et al., 2012) planned for launch in 2024 will provide similar observations over North America and Europe, respectively.

A study by Kim et al. (2023) evaluated GEMS L2 v1.0 total $NO_2$ VCD from November 2020 to January 2021 with four ground-based Pandora instruments, all located in Seosan, South Korea. They found correlation coefficients of 0.62-0.78 and an underestimation of the ground-based $NO_2$ measurements by the GEMS data set. Even though these four sites are relatively close together, they show different diurnal variations of $NO_2$, indicating that local transport or emissions have a significant influence. Zhang et al. (2023) evaluated their scientific POMINO-GEMS tropospheric $NO_2$ vertical column density (VCD) product with nine ground-based MAX-DOAS sites based on data from June-August 2021. The POMINO-GEMS product shows a modest correlation of 0.66 with the MAX-DOAS observations and a reasonable agreement between the diurnal variations of the two data products but cannot achieve the much better correlation of 0.83 of the POMINO-TROPOMI product and the MAX-DOAS observations. Oak et al. (2024) showed that the main reason for differences between the operational GEMS L2 v2.0 and the operational TROPOMI $NO_2$ product is an incorrect use of the vertical coordinates in the $NO_2$ profiles for the GEMS AMF computation. GEMS and TROPOMI products, both based on the same $NO_2$ vertical profile shapes, are in close agreement. Drivers of the diurnal variation of $NO_2$ observed by GEMS during winter and summer over Beijing and Seoul have been investigated by Yang et al. (2024). They used their own AMF and based their analysis on total $NO_2$ VCDs. With this, they found good agreement between the diurnal variations of total $NO_2$ VCDs in Pandora, GEMS, and GEOS-Chem. They used GEOS-Chem to interpret the observed variations and found that due to high emissions at the two urban sites, $NO_2$ accumulates over the day, which is offset by losses from chemistry and transport depending on season and wind speed. Edwards et al. (2024) used the GEMS L2 v2.0 tropospheric $NO_2$ VCD retrieval in combination with a chemical transport model to examine the $NO_2$ diurnal variation. Similar to Yang et al. (2024), they indicate different drivers for the diurnal variation on regional and local scales. Additionally, the model simulations show a high sensitivity to the assumed diurnal emission profile, especially on the local scale. A detailed analysis of the impacts from diverse chemical transport model simulations and different underlying $NO_x$ emissions on the GEMS $NO_2$ product has been conducted by Seo et al. (2024).

In this study, one year of tropospheric $NO_2$ VCDs retrieved by the operational GEMS L2 v2.0 product, the scientific GEMS IUP-UB v1.0 product, the operational TROPOMI product, and 11 ground-based DOAS instruments in South Korea are compared. Evaluating the GEMS tropospheric $NO_2$ VCD is important to assess and quantify its accuracy for use in surface concentration and emissions applications (e.g., Xu et al., 2023; Yang et al., 2023b). The 11 ground-based observation sites are located in different pollution regimes in South Korea, which provides the opportunity to observe and analyze different diurnal variations of $NO_2$. Including the TROPOMI product in the comparisons adds an already well-validated reference data set around noon. ECMWF reanalysis v5 (ERA5) wind data at 10 m altitude give valuable insights into the influence of transport effects on the diurnal variation. Using a full year of data allows to analyze the influence of seasonality and the weekday-weekend effect on the GEMS tropospheric $NO_2$ VCD. The scientific GEMS IUP-UB $NO_2$ retrieval gives the possibility to change a priori assumptions such as the surface reflectivity and investigate its influence. Also the influence of different stratospheric corrections on the tropospheric $NO_2$ products is investigated.

The instruments and data sets included in this study are described in Sect. 2. After a first comparison of one month of averaged GEMS L2 v2.0, GEMS IUP-UB v1.0, and TROPOMI v02.04.00 tropospheric $NO_2$ VCDs maps in Sect. 3, one year of satellite tropospheric $NO_2$ VCDs is evaluated by comparisons with the tropospheric $NO_2$ VCD data set of the ground-based network

distributed within South Korea (see Sect. 4.2) and car DOAS observations (see Sect. 4.3). In Sect. 5 the diurnal variations of the GEMS IUP-UB $NO_2$ VCDs and the ground-based observations are analyzed. Factors such as seasonality, wind speed, transport processes, and the weekday-weekend effect that influence the tropospheric $NO_2$ VCD are investigated to better understand the origin of the observed diurnal variations. Possible reasons for deviations between GEMS and ground-based observations, such as the stratospheric correction, the surface reflectivity, and viewing geometry, are discussed in Sect. 5.4. A summary and conclusions are provided in Sect. 6.

## 2 Instruments and data sets

In this study, data from two measurement campaigns in South Korea are used: The GEMS Map of Air Pollution (GMAP) 2021 and the Satellite Integrated Joint Monitoring of Air Quality (SIJAQ) 2022 campaigns (https://www.sijaq.org). The main campaign periods took place from October 2021 to November 2021 and May 2022 to August 2022. Some instruments were also operated between the main campaign periods and beyond. Analyses of this study focus on measurements taken between October 2021 and October 2022. One key aspect of these campaigns was to gather measurements for the validation and improvement of GEMS data, to better understand uncertainties and error sources in the satellite products, to support further improvement of the satellite retrieval algorithms, and to apply GEMS data for the characterization of air pollution.

Instruments from several teams participated in the campaigns. Measurements were delivered by stationary MAX-DOAS and Pandora instruments, as well as mobile car DOAS instruments. More details about the different instruments are provided below in Sect. 2.3 and 2.4. During the GMAP 2021 campaign, measurements were focused on the Seoul Metropolitan Area (SMA), having a population of 26 million, one of the largest and most polluted metropolitan regions worldwide. During the SIJAQ 2022 campaign, measurements were additionally performed in the southern part of South Korea. This region includes Busan, the second largest city in South Korea, and Ulsan, an important industrial center. Figure 1 shows GEMS observations of tropospheric $NO_2$ VCDs over South Korea, indicating several pollution hot spots and the locations of the stationary instruments. The combination of stationary and mobile measurements makes a comprehensive validation of GEMS data possible. The stationary MAX-DOAS measurements are located in different pollution regimes and provide daily measurements with a high temporal resolution, but are restricted in spatial coverage to the area around the site, where each instrument is located. The car DOAS measurements lack temporal resolution but are operated such that they make measurements within several satellite ground pixels in different regions. This enables a variety of pollution levels and thus air quality conditions to be investigated. Table 1 lists all instruments involved in this study.

### 2.1 Geostationary Environmental Monitoring Spectrometer (GEMS)

GEMS is a step-and-stare UV-visible imaging spectrometer onboard the satellite GK2B (Geostationary Korea Multi-Purpose Satellite 2), launched into geostationary orbit on 18 February 2020. It is the first geostationary mission to monitor air quality hourly during the daytime. With its location at a longitude of 128.2°E over the Equator, GEMS covers a large part of Asia (5°S-45°S and 75°E-145°E). The ground pixels have a nominal resolution of approximately $3.5\,\mathrm{km} \times 8\,\mathrm{km}$ over Seoul. GEMS

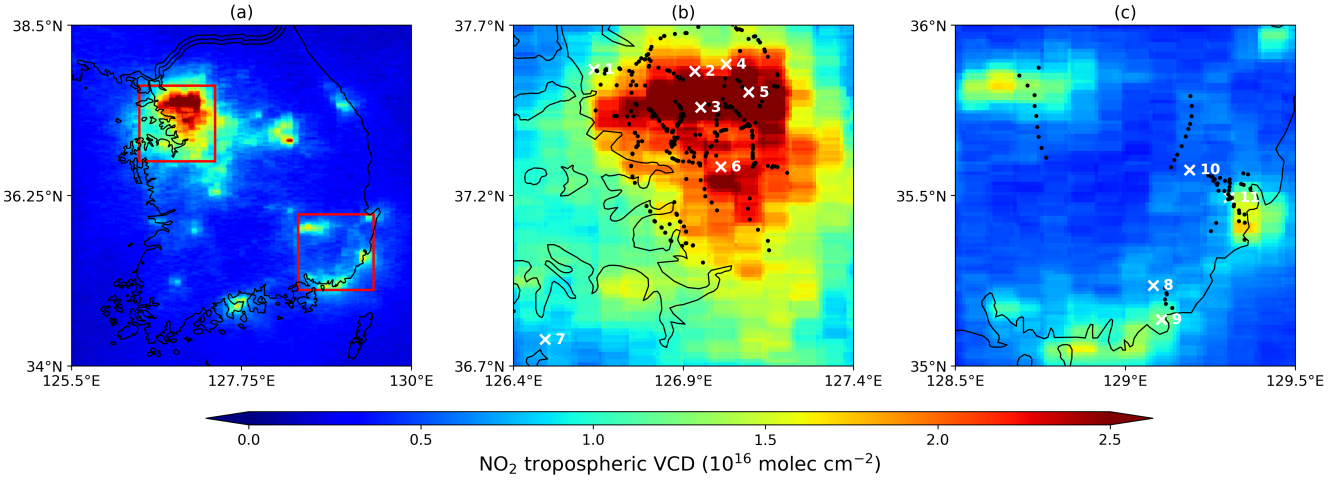


**Figure 1.** Maps of monthly mean $NO_2$ tropospheric VCDs for South Korea. Panel (a) shows GEMS IUP-UB v1.0 observations in October 2021 around 13:45 Korean Standard Time (KST) (04:45 UTC). Panel (b) is a zoom into the SMA region indicated by the upper red rectangle in panel (a). Panel (c) is a zoom into the southeast, indicated by the lower red rectangle in panel (a). The white crosses show the locations of the ground-based measurement sites. The different instruments are listed together with the number given in Table 1. Black dots indicate locations of car DOAS observations used for GEMS validation.

is operated in 4 scan modes and allows up to 10 observations per day over the eastern part of the covered area, which includes South Korea. Due to shorter days, the number of possible observations is reduced to 8 in March and October and is further limited to a maximum of six observations in winter. The GEMS spectrometer covers the wavelength range of 300-500 nm and has a spectral resolution of 0.6 nm. The measurements yield column amounts of $O_3$, $NO_2$, $SO_2$, HCHO, CHOCHO, and also aerosol and cloud information (Kim et al., 2020). We use the tropospheric $NO_2$ VCD of the operational GEMS L2 v2.0 product and the scientific GEMS IUP-UB v1.0 product, which are described below.

#### 2.1.1 Operational GEMS L2 tropospheric $NO_2$ VCD product v2.0

The operational GEMS L2 tropospheric $NO_2$ VCD product v2.0 was reprocessed for the entire mission and is distributed by the National Institute of Environmental Research, NIER (https://nesc.nier.go.kr/en/html/cntnts/91/static/page.do). Data are available from 2021 onward. GEMS irradiance data are wavelength calibrated using the pre-launch spectral response function. A single wavelength calibration is applied across all rows. $NO_2$ slant column densities (SCDs) are retrieved from Level 1 spectra using a DOAS fit in the fitting window of 432-450 nm. Using a lookup table of altitude-dependent air mass factors (AMFs) and model-based vertical profile shapes, the $NO_2$ SCDs are converted into $NO_2$ VCDs. In v2.0, the WRF-Chem + CAM-Chem model used in v1.0 (Lee et al., 2020), was replaced with the GEOS-Chem model, which has a spatial resolution of $0.25\,^\circ \times 0.3125\,^\circ$. The altitude-dependent AMFs from the radiative transfer model VLIDORT (Spurr, 2006) are tabulated as a function of the solar zenith angle (SZA), the viewing zenith angle (VZA), the relative azimuth angle (RAA), surface

**Table 1.** List of instruments included in this study with location, observation geometry, VCD retrieval information, and period of observation. MAX-DOAS BIRA Seoul (4) and MAX-DOAS BIRA Suwon (6) sites are using the same instrument, which was moved from Suwon to Seoul in December 2021.

| Instrument | Location/Platform | Observation geometry | VCD retrieval | Available data |
|---|---|---|---|---|
| GEMS | GEO-KOMPSAT-2B | Step-and-stare, nadir | L2 v2.0 and IUP-UB v1.0 | 6-10 times/day |
| TROPOMI | Sentinel-5P | Push-broom, nadir | RPRO/OFFL v2.4.0 | 1-2 times/day (~13:30 KST) |
| MAX-DOAS IUP-UB Incheon (1) | Incheon (37.57° N, 126.64° E) | Multi-axis | FRM4DOAS 01.01 MMF | Oct 2021 - Oct 2022 |
| Pandora 54 Yonsei (2) | Seoul (37.56° N, 126.93° E) | Multi-axis | PGN rnvh3.1-8 | Oct 2021 - Oct 2022 |
| Pandora 149 SNU (3) | Seoul (37.46° N, 126.95° E) | Multi-axis | PGN rnvh3.1-8 | Oct 2021 - Oct 2022 |
| MAX-DOAS BIRA Seoul (4) | Seoul (37.59° N, 127.03° E) | Multi-axis | FRM4DOAS 01.01 MMF | Dec 2021 - May 2022 |
| MAX-DOAS MPIC Seoul (5) | Seoul (37.50° N, 127.09° E) | Multi-axis | FRM4DOAS 01.01 MMF | Oct 2021 - Aug 2022 |
| MAX-DOAS BIRA Suwon (6) | Suwon (37.28° N, 127.01° E) | Multi-axis | FRM4DOAS 01.01 MMF | Oct 2021 - Dec 2021 |
| Pandora 164 Seosan (7) | Seosan (36.78° N, 126.49° E) | Multi-axis | PGN rnvh3.1-8 | Oct 2021 - Oct 2022 |
| Pandora 20 Busan (8) | Busan (35.24° N, 129.08° E) | Multi-axis | PGN rnvh3.1-8 | Oct 2021 - Oct 2022 |
| MAX-DOAS MPIC Busan (9) | Busan (35.14° N, 129.11° E) | Multi-axis | FRM4DOAS 01.01 MMF | Jun 2022 - Aug 2022 |
| Pandora 150 Ulsan (10) | Ulsan (35.57° N, 129.19° E) | Multi-axis | PGN rnvh3.1-8 | Oct 2021 - Oct 2022 |
| MAX-DOAS IUP-UB Ulsan (11) | Ulsan (35.49° N, 129.31° E) | Multi-axis | FRM4DOAS 01.01 MMF | Jun 2022 - Oct 2022 |
| IUP car DOAS | Mobile car | Zenith-sky | | campaign based |
| MPIC car DOAS | Mobile car | Zenith and 22° | | campaign based |
| BIRA car DOAS | Mobile car | Zenith-sky | | campaign based |

albedo, terrain height, temperature and pressure profiles, and aerosol parameters. The aerosol optical thickness (AOD), the single scattering albedo (SSA), and the aerosol layer height (ALH) are taken from GEMS L2 data. Since v2.0, the surface albedo is based on GEMS L2 surface reflectance data instead of the OMI climatology. The cloud correction of the AMF uses a linear combination of a clear-sky and a cloudy AMF, weighted by the cloud radiance fraction. The separation of the total $NO_2$ VCD into its stratospheric and tropospheric parts is based on Bucsela et al. (2013), using GEOS-Chem model data for the tropospheric $NO_2$ column a priori and to mask high pollution regions.

To remove problematic retrievals and cloudy scenes, we use only GEMS data with a final algorithm flag of 0 and a cloud fraction < 0.3. The product provides the 'root_mean_square_error' resulting from the $NO_2$ fit but does not include errors from other retrieval aspects. Therefore, we estimate the tropospheric $NO_2$ VCD error based on the assessment done for the TROPOMI product with a typical value over continental polluted areas of $\pm 25\,\%$, which is dominated by the uncertainties in the AMF calculation (van Geffen et al., 2022).

### 2.1.2 Scientific GEMS IUP-UB tropospheric $NO_2$ VCD product v1.0

As part of the preparation for the European geostationary instrument on the satellite Sentinel-4, a scientific GEMS $NO_2$ product has been developed at the Institute of Environmental Physics at the University of Bremen (IUP-UB). The GEMS L1 spectra are analyzed using the DOAS technique in a larger fitting window from 405–485 $\mathrm{nm}$ and in comparison to the operational GEMS

L2 product, data are corrected for instrument polarization sensitivity and scene inhomogeneity, and are de-striped. This results in less noise, a reduction of scatter, and improves the consistency with other products (TROPOMI, GOME-2) using similar large fitting windows. The retrieved SCDs are corrected for the stratospheric contribution based on the STRatospheric Estimation Algorithm from Mainz (STREAM, Beirle et al. (2016)). Tropospheric SCDs are converted into tropospheric VCDs with $NO_2$ a priori profile shapes from the TM5 chemical transport model (Williams et al., 2017) and a lookup table of altitude-dependent AMFs computed with the radiative transfer model SCIATRAN (Rozanov et al., 2014). The TM5 model has a spatial resolution of $1\,^\circ \times 1\,^\circ$. The altitude-dependent AMFs are tabulated as a function of SZA, VZA, RAA, surface albedo, and surface height. The surface albedo is based on the TROPOMI Lambertian equivalent reflectivity (LER) climatology (Tilstra et al., 2023). To evaluate the influence of the surface albedo, an additional version was created using the GEMS L2 surface reflectance data. The AMF cloud correction is based on the independent pixel approximation and uses recalculated cloud fractions and the cloud pressure from the GEMS L2 cloud product. The cloud fractions were computed from recalculated GEMS top of atmosphere (TOA) reflectances based on GEMS radiances and recalibrated irradiances by comparison with TOA reflectances modelled by SCIATRAN. In the current version of the algorithm, no aerosol correction is included. More details about the scientific GEMS IUP-UB tropospheric $NO_2$ v1.0 retrieval will be provided in an upcoming publication by Richter et al.

Problematic retrievals and cloudy scenes with cloud radiance fractions of more than 50 % are removed using only observations with a quality assurance value (qa_value) above 0.75. The quality flagging system is similar to that used in the operational TROPOMI product. However, the GEMS IUP-UB product does not yet have full error propagation and contains the 'nitrogendioxide_tropospheric_vertical_column_density_uncertainty_random', which, as in the operational product, only contains the random error from the fit. The tropospheric $NO_2$ VCD error is estimated based on the same $\pm 25\,\%$ assumption.

### 2.2 TROPOspheric Monitoring Instrument (TROPOMI)

TROPOMI is a hyperspectral imaging spectrometer onboard the sun-synchronous near polar-orbiting satellite Sentinel-5P (S5P), launched in October 2017 (Veefkind et al., 2012). With its measurements in the UV, visible, and IR spectral regions, TROPOMI can monitor several atmospheric trace gases as well as clouds and aerosols. We use the tropospheric $NO_2$ VCD product retrieved from measurements in the visible channel (400-496 $\mathrm{nm}$). The ground pixel sizes are approximately 3.5 $\mathrm{km}$ $\times$ 5.5 $\mathrm{km}$ in the middle of the swath. With orbit times of around 100 $\mathrm{min}$ and a wide swath of approximately 2600 $\mathrm{km}$, TROPOMI has nearly global coverage and usually one to two overpasses per day in the mid-latitudes. Over the campaign region, TROPOMI provides observations between 12:28 and 14:40 Korean Standard Time (KST).

#### 2.2.1 TROPOMI tropospheric $NO_2$ VCD product v02.04.00

The latest TROPOMI tropospheric $NO_2$ product, reprocessed for the entire mission, uses processor version 02.04.00. The v02.04.00 product was generated operationally from 17 June 2022 to 12 March 2023. We are using the offline (OFFL) as well as the reprocessed (RPRO) data of this version, which is available from the Sentinel-5P Pre-Operations Data Hub (last access: 21 February 2022). The following processor versions had only minor bug fixes and have not yet been applied to the full data set (Eskes and Eichmann, 2023). The Level 1b version 2.1 spectra are analyzed with the DOAS technique in a fitting window

of 405-465 nm to retrieve $NO_2$ SCDs. The retrieved SCDs are separated into their stratospheric and tropospheric parts with $NO_2$ vertical profile information from the $1° \times 1°$ TM5 global chemistry transport model and a data assimilation system that assimilates TROPOMI SCDs. Using a lookup table of altitude-dependent AMFs and actual daily TM5 $NO_2$ vertical profile shapes, the resulting tropospheric SCDs are converted into tropospheric VCDs. The altitude-dependent AMFs are a function of SZA, VZA, RAA, surface albedo, surface pressure, and (mid-level) atmospheric pressure. Since v02.04.00, the surface albedo in the $NO_2$ spectral fitting window and in the cloud pressure retrieval is based on the TROPOMI directionally dependent LER (DLER) climatology (Tilstra et al., 2023). The cloud radiance fraction is retrieved from the $NO_2$ spectral region at 440 nm. The cloud pressure retrieval is based on the FRESCO-wide algorithm in the NIR spectral range. In the AMF, both clouds and, indirectly, aerosol loads are accounted for by using a linear combination of a clear-sky and a cloudy AMF, weighted by the cloud radiance fraction (van Geffen et al., 2022).

To remove problematic retrievals, we are using only observations with the recommended qa_value above 0.75. This also removes scenes with cloud radiance fractions in the $NO_2$ window of more than 50 % (Eskes and Eichmann, 2023). The TROPOMI $NO_2$ product contains the data field 'nitrogendioxide_tropospheric_column_precision', which provides the error estimate originating from the $NO_2$ fit and other retrieval aspects that are dominated by the uncertainty in the tropospheric AMF of 25 %.

### 2.3 MAX-DOAS observations and data sets

The satellite tropospheric $NO_2$ VCDs are compared to collocated MAX-DOAS tropospheric $NO_2$ VCDs. We use data from MAX-DOAS instruments at six sites in South Korea. Four sites were located in the northern campaign region and two in the southeastern campaign region (see Table 1). Not all of them have been operated over the whole year of measurements. The data availability for the satellite validation can be seen in the Appendix Fig. A8. The ground-based MAX-DOAS instruments measure the UV-visible scattered sunlight in several azimuthal directions and elevations. The tropospheric $NO_2$ VCDs used in this study were retrieved by applying the Mexican MAX-DOAS Fit (MMF; Friedrich et al. (2019)) inversion algorithm using the FRM4DOAS (v01.01, https://frm4doas.aeronomie.be/) settings and setup (Hendrick et al., 2016). The product is quality filtered using only data with a recommended 'qa_flag_no2' of 0 and 1. This quality flag uses additionally the Mainz profile algorithm (MAPA; Beirle et al. (2019b)) data in the quality check. Details about the implemented algorithms and quality flagging approaches will be provided in an upcoming publication by Hendrick et al. (expected 2024). To ensure comparability between the MAX-DOAS instruments from different institutes, an intercomparison period was conducted at the beginning of the campaign. During this period, all instruments, except for the MAX-DOAS IUP-UB Ulsan, were operated at the same location. The comparisons show very good correlations between the instruments. The inter-comparison results will be presented in the upcoming publication by Hendrick et al. (expected 2024).

The Pandonia Global Network (PGN, https://www.pandonia-global-network.org) is a network of ground-based UV-visible spectrometers called Pandora, which focuses on total column observations from direct sun measurements, but also provides tropospheric column observations when operated in multi-axis mode. We use data from the five Pandora instruments, located in South Korea that are operated in the multi-axis mode. Three of them are located in the northern campaign region, and two

are in the southeastern region. Data are processed as part of the PGN Pandonia Global Network (last access: 4 February 2023). All data are on the processor version 1.8 and retrieval version nvh3. We filter data which are flagged as unusable (20, 21, and 22) and additionally for wrms (normalized rms of fitting residuals weighted with independent uncertainty) larger than 0.002. Details on the retrieval of the tropospheric $NO_2$ VCD and the respective uncertainty can be found in Cede (2021).

### 2.4 Car DOAS instruments and data sets

During the GMAP 2021 and SIJAQ 2022 main campaign periods, mobile car DOAS measurements were performed by instruments of the IUP-UB, the Max Planck Institute for Chemistry in Mainz (MPIC), and the Royal Belgian Institute for Space Aeronomy (BIRA). To achieve high spatial resolution over the covered area, the majority of measurements was taken in zenith-sky with some off-zenith measurements. Instruments were operated in both campaign regions and synchronized to the GEMS schedule to cover several GEMS observations throughout the day. Compared to the stationary data, the car measurements have the advantage that they cover larger and more diverse areas. The car DOAS data analysis was done independently by the operating institutes. More details about the car DOAS instruments and the tropospheric $NO_2$ VCD retrieval can be found in Lange et al. (2023).

## 3 Satellite tropospheric $NO_2$ product comparison

Before comparing the satellite tropospheric $NO_2$ VCD products with ground-based measurements, an assessment of the three products based on maps of monthly averaged tropospheric $NO_2$ VCDs provides a first assessment of the differences between the two GEMS $NO_2$ products and the TROPOMI product. Figure 2 shows maps of the tropospheric $NO_2$ VCDs for South Korea from GEMS L2 v2.0 (a), GEMS IUP-UB v1.0 (b), and TROPOMI v02.04.00 (c) observations in October 2021. For better comparison, the two GEMS data sets are averaged only for the 13:45 KST (04:45 UTC) observation, which is close to the TROPOMI overpass between 12:28 KST and 14:37 KST. Data are sampled at 0.01° resolution. As the AMF of the GEMS L2 v2.0 $NO_2$ product is not interpolated in space, the map of the tropospheric $NO_2$ VCDs (a) shows box structures with boxes of the same size as the spatial resolution of the GEOS-Chem model.

All three maps show elevated $NO_2$ concentrations centered over the SMA and several smaller elevated $NO_2$ regions with the Danyang county, including Jecheon and a mining area in the mid-north, Donghae on the east coast, Gwangyang in the south, and Daegu, Pohang, Ulsan, and Busan in the southeast. These regions of elevated $NO_2$ show the highest values in the GEMS L2 tropospheric $NO_2$ VCD product, especially over the SMA, followed by the GEMS IUP-Bremen product and the lowest values in the TROPOMI product. Additionally, we note that the background $NO_2$ is similar in the TROPOMI and GEMS IUP-UB products but significantly higher in the GEMS L2 product. This difference in the background $NO_2$ can be caused by the different stratospheric corrections used in the three products (GEOS-Chem with GEMS data assimilation, STREAM, and TM5 with TROPOMI data assimilation). These are discussed further in Sect. 5.4. The influence of the stratospheric correction will be visible most prominently in the evaluation with the ground-based data for stations located in low-polluted regions such as the Pandora Ulsan, which is located at the Ulsan National Institute of Science and Technology, several kilometers outside

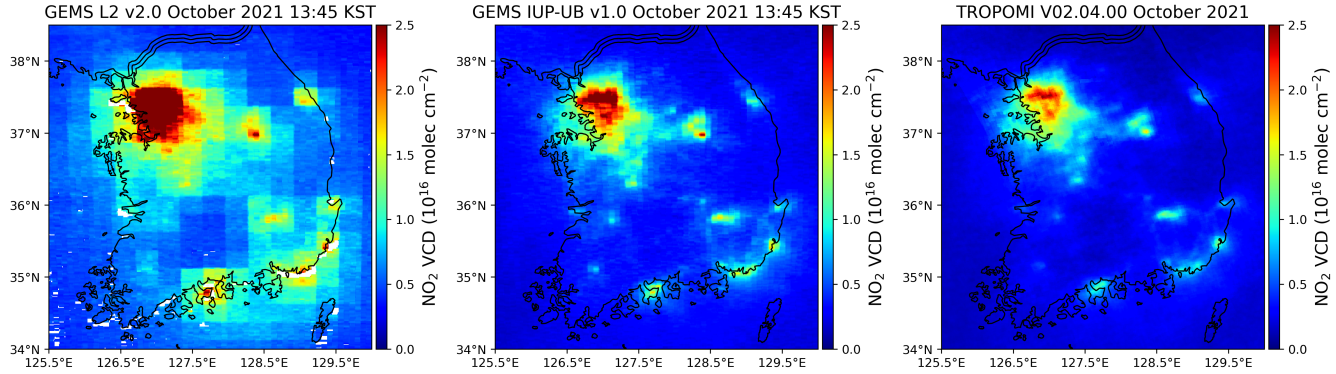


**Figure 2.** Maps of $NO_2$ tropospheric VCD for South Korea from GEMS L2 v2.0 (a), GEMS IUP-UB v1.0 (b), and TROPOMI v02.04.00 (c) observations in October 2021. The GEMS data sets are averaged for the 13:45 KST (04:45 UTC) observation close to the TROPOMI overpass. All data sets are cloud and quality filtered.

the city and industrial area of Ulsan, or the Pandora Seosan (instruments 10 and 7, see Fig. 1). The map of the TROPOMI $NO_2$ product appears the most smoothed, caused by the orbital cycle of 16 days and the resulting oversampling. Since GEMS maintains a constant ground pixel pattern for each of the four scan modes, there is no oversampling and smoothing, which makes the sampling pattern visible in the GEMS averages. Missing data in the GEMS L2 v2.0 $NO_2$ product, which are mainly visible in coastal regions, are caused by the product's quality filter.

## 4 Evaluating satellite tropospheric $NO_2$ VCD with ground-based data

### 4.1 Collocation criteria - method

Stationary ground-based tropospheric $NO_2$ VCDs are averaged within $\pm$ 20 min of the satellite overpass and compared to the closest satellite pixels extracted within a radius of 5 km around the station sites. Other criteria for co-location were tested, e.g., including larger areas, area averaging, and considering the ground-based instruments VAA during the satellite overpass. Some of the results are shown in Fig. A3 in the Appendix. The results are either slightly worse or not significantly better than the nearest pixel approach. This is in contrast to Dimitropoulou et al. (2020), who showed significant improvements in slope and correlation when considering the directional dependency for a comparison of TROPOMI and MAX-DOAS observations in Uccle, Belgium. Therefore, further investigations are required into why the comparisons in South Korea behave differently. All linear regression statistics in this study are calculated with orthogonal distance regression (ODR) to take into account the error in both evaluated and reference measurements. The correlation between the evaluated and reference measurements is described by the Pearson correlation coefficient (r). Additionally, the median relative difference (mrd) is calculated by the following convention:

$$\text{median relative difference}(\%) = \frac{\text{(evaluated - reference)}}{\text{reference}} \cdot 100 \quad (1)$$

The evaluated measurements are the satellite tropospheric $NO_2$ VCDs. The reference measurements are either the stationary ground-based or the mobile car DOAS tropospheric $NO_2$ VCDs in Sect. 4.3.

### 4.2 Evaluating satellite tropospheric $NO_2$ VCD with MAX-DOAS and Pandora

The large data set of ground-based instruments distributed in South Korea is used to evaluate the satellite tropospheric $NO_2$ VCD product. Scatter plots of all coincident satellite and stationary ground-based measurements are shown in Fig. 3 for the GEMS L2 (panel a), the GEMS IUP-UB (panel b), and the TROPOMI (panel c) $NO_2$ tropospheric VCD products. Since all 6-10 observations per day are considered in the comparisons of the GEMS products to the ground-based data set, there are 8388 coincident measurements for the GEMS L2 and 12959 for the GEMS IUP-UB product, which is many more than for the TROPOMI product with 1703. A comparison limited to the TROPOMI overpass time between 12:28 KST and 14:37 KST is shown in the Appendix Fig. A1. The difference in the number of coincident measurements between the GEMS L2 and the

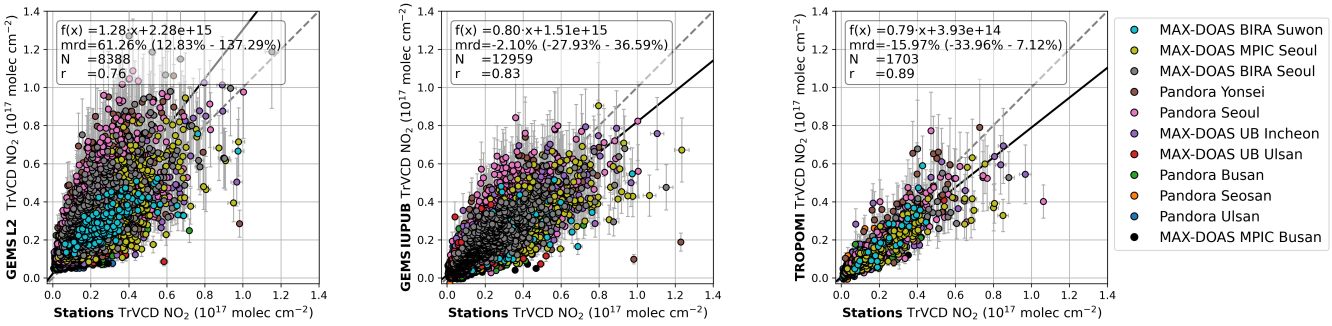


**Figure 3.** Scatter plots of GEMS L2 (a), GEMS IUP-UB (b), and TROPOMI (c) $NO_2$ tropospheric VCDs vs. co-located ground-based $NO_2$ tropospheric VCDs. The ground-based observations are considered co-located if they are taken within $\pm$ 20 min around the satellite observation. Measurements within this period are averaged and matched to the closest satellite observation within a radius of 5 km around the station site. The error bars represent the tropospheric $NO_2$ VCD error. Points are colored according to the corresponding ground-based instrument. The dashed gray line indicates the 1:1 line. The solid black line represents the orthogonal distance regression.

GEMS IUP-UB product is mainly caused by the stricter quality filter of the GEMS L2 product. Limiting the filter process of the GEMS L2 product on the cloud filter only, results in a more comparable number of data points.

The GEMS L2 and ground-based tropospheric $NO_2$ VCDs have a Pearson correlation coefficient of r = 0.76, with a slope of 1.28, a median relative bias of +61 %, and an offset of $2.28 \times 10^{15}$ molec cm$^{-2}$. This overestimation is in contrast to the underestimation visible in the GEMS IUP-UB and TROPOMI $NO_2$ products. Potential explanations for this different bias, such as the surface reflectivity used for the AMF determination, the stratospheric correction and the consideration of aerosol parameters, are further discussed in Sect. 5.4. The GEMS IUP-UB as well as the TROPOMI product show a slight underestimation, with slopes of 0.80, respectively 0.79, and a median bias of -2 % and -16 %. A similar magnitude of underestimation of satellite tropospheric $NO_2$ VCDs relative to ground-based observations has been observed in many validation studies for satellite data

sets (e.g., Ma et al., 2013; Verhoelst et al., 2021) and is often explained by local $NO_2$ hot spots that are not resolved in the satellite data and the a priori fields used for the AMF calculations. Another reason is the missing aerosol correction in these satellite products. When binning the median relative differences of the GEMS IUP-UB and MAX-DOAS comparison by the AOD, determined in the FRM4DOAS MAX-DOAS analysis, an increasing bias is observed with an increase in the AOD (see Appendix Fig. A2). This was similarly observed for a comparison of tropospheric $NO_2$ VCDs of MAX-DOAS and TROPOMI (Lambert et al., 2023).

The GEMS IUP-UB product, considering all observations per day, has a good correlation with a coefficient of 0.83 but is more scattered than the TROPOMI product, which is limited to its noon observation time. To investigate whether the better correlation of the TROPOMI product is attributed to the data itself or the timing of the satellite overpass, all data sets were limited to the period corresponding to TROPOMI overpasses, see Appendix Fig. A1. For both, the GEMS L2 and the GEMS IUP-UB product, the time limit increases the slope and median bias slightly and reduces the scatter. This indicates larger deviations between the GEMS and ground-based tropospheric $NO_2$ VCDs in the morning and/or afternoon, which will be further analyzed by comparing the diurnal variation in Sect. 5.

When separating the comparison of the satellite and ground-based observation into the individual sites, quite some differences can be observed between the individual sites. Figure 4 shows box-and-whisker plots for the three satellite $NO_2$ products and all stations summarizing the bias and spread of the differences. For the GEMS L2 product, differences between the individual

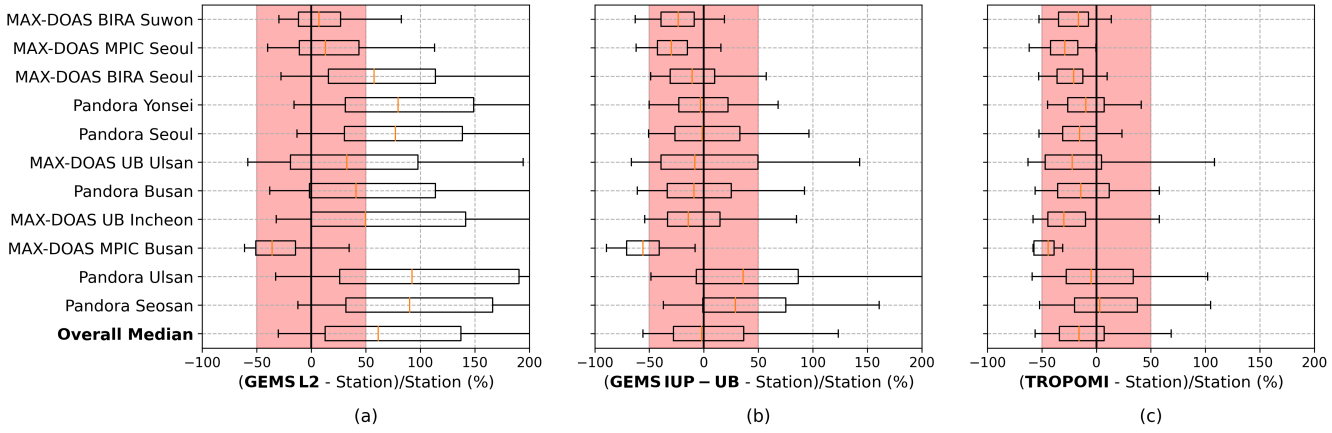


**Figure 4.** Box-and-whisker plots summarizing the bias and spread of the difference between the (a) GEMS L2, (b) GEMS IUP-UB, (c) the TROPOMI and the individual ground-based tropospheric $NO_2$ VCDs. Stations are ordered from bottom to top by increasing median ground-based tropospheric VCD. The orange line inside the box represents the median relative difference. Box bounds mark the 25 and 75 % quantiles. Whiskers represent the 5 and 95 % quantiles. The red-shaded area represents a bias of $\pm$ 50 %.

sites are even larger due to the dependence on the AMF box in which the station is located (see Fig. 2). The large negative bias for the MAX-DOAS MPIC Busan site is visible in all product comparisons and is possibly caused by its location close to the coast (<500 m) and the associated inhomogeneities. The sea-land breeze circulation can create complex horizontal and vertical

gradients in atmospheric composition, which are difficult to resolve in a priori profiles used for satellite retrievals (e.g., Souri et al., 2023). Furthermore, the measurements of this instrument are performed in an azimuth direction of 253°, which crosses the port of Busan, a local source of $NO_x$. In general, there is a slight tendency to larger biases for more polluted sites while less-polluted sites show differences closer to 0. These findings are similar to the validation results from Verhoelst et al. (2021) on TROPOMI $NO_2$ data. The positive bias in the GEMS IUP-UB for the Pandora Ulsan and the Pandora Seosan, both less polluted sites, could indicate an underestimation of the stratospheric contribution at these sites.

The overall bias (median of all satellite and station pair differences) is 61 % (13 % - 137 % interquartile range) for the GEMS L2 product, -2 % (-28 % - 37 %) for the GEMS IUP-UB product, and -16 % (-34 % - 7 %) for the TROPOMI product. A comparison by Lambert et al. (2023) based on tropospheric $NO_2$ VCDs of the Network for the Detection of Atmospheric Composition Change (NDACC) MAX-DOAS data from 29 stations and TROPOMI data of v2.4.0 and v2.5.0 from May 2018 to November 2023 shows a median bias of -28 % and for a subset of eight MAX-DOAS stations in the TROPOMI Validation Data Analysis Facility Automated Validation Server (VDAF-AVS) of -17.5 %. Thus somewhat larger than for the data set analyzed here. For the GEMS IUP-UB and the TROPOMI product, the overall and the individual biases, except for the MAX-DOAS MPIC Busan, are within the typical mission requirement of a maximum bias of 50 % (van Geffen et al., 2022). In general, the GEMS IUP-UB product and the TROPOMI product show good agreement in the individual biases, which is improved when limiting the GEMS IUP-UB product comparisons to the TROPOMI overpass time. Scatter plots of the satellite products vs. the co-located ground-based data for the 11 individual stations can be found in the Appendix (Fig. A4, Fig. A5, Fig. A6).

### 4.3 Comparison of GEMS IUP-UB and car DOAS observations

The car DOAS tropospheric $NO_2$ VCDs are used, in addition to the stationary ground-based observations, to evaluate the GEMS IUP-UB tropospheric $NO_2$ VCDs. The IUP, MPIC, and BIRA car DOAS instruments were operated in the two campaign regions. Considering that the car DOAS data used for this comparison were analyzed independently by the different groups and with only partly harmonized retrieval methods with different assumptions, the data show good agreement and provide an additional data set for the evaluation of GEMS data. The locations of the car DOAS observations are displayed in Fig. 1. Compared to the stationary data, they can cover larger and more diverse areas, which is reflected in the large range of $NO_2$ values shown in Fig. 5. The scatter plot shows GEMS IUP-UB tropospheric $NO_2$ VCDs vs. co-located car DOAS $NO_2$ tropospheric VCDs. The car DOAS data are compared to the GEMS pixel in which they were measured, averaged $\pm$ 20 min around the GEMS observation. In total, 1146 pairs of coincident measurements are considered, of which 272 were taken during the TROPOMI overpass time window. The comparison between the GEMS IUP-UB and the car DOAS data shows a good correlation with a correlation coefficient of 0.87. The slope of 0.7 and a median relative bias of -30 % indicate a larger negative bias than the comparison with the stationary ground-based data set. This larger underestimation of the GEMS IUP-UB product may be caused by the bias of the larger proportion of high $NO_2$ tropospheric VCDs, which was already visible from the evaluation by individual stations for the more polluted sites. Horizontal bars indicate the 10th and 90th percentile of car DOAS observations within the GEMS pixel and $\pm$ 20 min time intervals to illustrate the spatiotemporal variability. These bars can become relatively large, indicating the considerable temporal and spatial variability of tropospheric $NO_2$ even within the

GEMS pixel. Further investigations based on the car DOAS observations can provide more insights into the representativeness of observations and the natural variability of $NO_2$.

## 5 Diurnal variation of GEMS and ground-based tropospheric $NO_2$ VCDs

GEMS is the first geostationary instrument able to observe the diurnal variation of $NO_2$. We assess the agreement between the diurnal variation observed by GEMS and that observed by the ground-based instruments. Interpreting the observed diurnal variations and their differences is difficult as they are driven by emissions, the chemistry of $NO_x$, and transport processes. These factors vary with season, wind speed, transport processes, and weekday-weekend effects, and are analyzed in more detail in the following sections.

### 5.1 Seasonality

Figure 6 shows the observed diurnal variation divided into winter (DJF), spring (MAM), summer (JJA), and autumn (SON) from the GEMS IUP-UB and the station's data sets for those stations which were operated over the whole year, six out of the eleven stations. At the sites within the SMA (Incheon, Yonsei, Seoul), mean tropospheric $NO_2$ VCDs are larger than at the other sites, and the diurnal variation can be quite different between the individual sites (see also Chong et al. (2018)) and

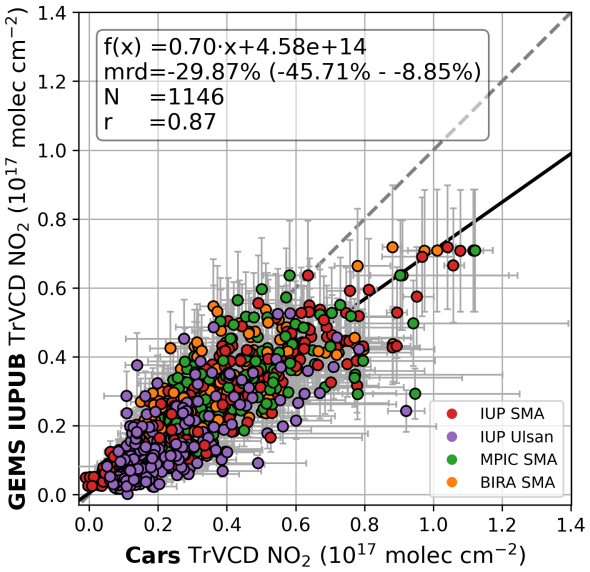


**Figure 5.** Scatter plot of GEMS IUP-UB tropospheric $NO_2$ VCDs vs. co-located car DOAS $NO_2$ tropospheric VCDs. The car DOAS observations are considered co-located if they are taken $\pm$ 20 min around the time of the GEMS measurement within the satellite pixel. Each point is colored by the respective car DOAS instrument. Vertical bars represent the tropospheric $NO_2$ VCD error. Horizontal bars are the 10th and 90th percentile to illustrate the spatiotemporal variability.

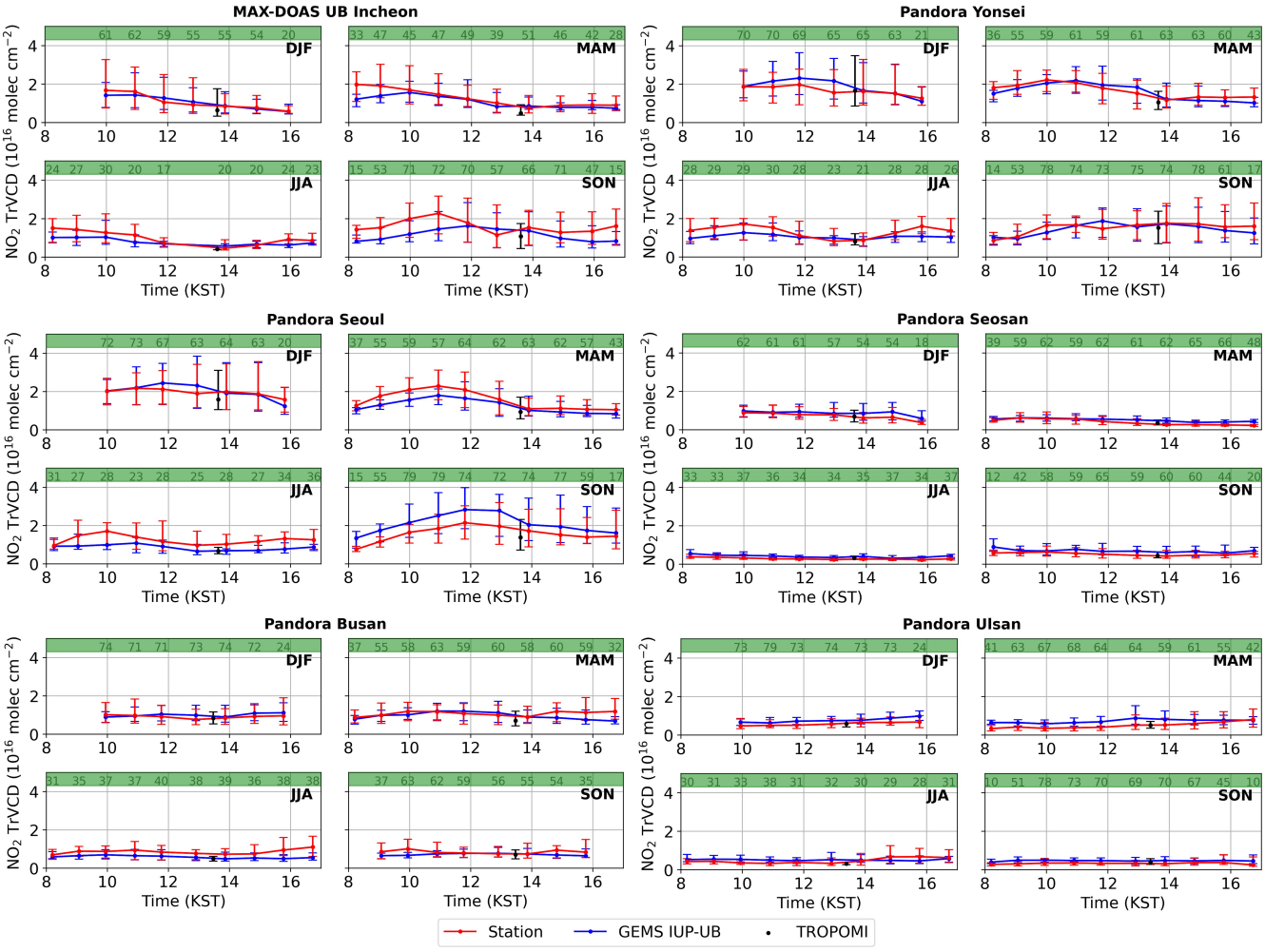


**Figure 6.** Diurnal variation of median tropospheric $NO_2$ VCDs from the GEMS IUP-UB product (blue) and ground-based stations (red) for the individual seasons (DJF, MAM, JJA, SON). The TROPOMI observation is added in black. Station names can be found in the individual titles. Vertical bars represent the 25 and 75 % quantiles of the MAX-DOAS and GEMS observations. Numbers in the green bar represent the number of contributed observations. Plots for the GEMS L2 product can be found in the Appendix Fig. A7.

differ additionally between the seasons. However, the overall behavior of the GEMS IUP-UB and the ground-based data are very similar. The low-polluted sites, the Pandora Seosan and the Pandora Ulsan, show little diurnal variation and a high bias of the GEMS IUP-UB tropospheric $NO_2$ VCD, which is relatively stable over the day. For the Pandora Seoul site, the GEMS IUP-UB product overestimates the station columns in autumn, but both show very similar diurnal variation. The other sites show the best agreement around noon from around 11 to 14 KST. Several stations show deviations in the morning and late afternoon, where the GEMS IUP-UB product often underestimates the station values, which is for example visible prominently for the MAX-DOAS UB Incheon in summer and autumn, and the Pandora Yonsei in summer. For the Pandora Busan site, the

underestimation of the GEMS IUP-UB product is strongest in the late afternoon, especially during spring and summer. These deviations during the morning and late afternoon observations are also visible for the GEMS L2 product (see Appendix Fig. A7), but less pronounced as it is generally high biased. These differences for observations at larger SZA can be explained by a lower sensitivity and more uncertain AMFs for these scenes, which is amplified for larger aerosol loads and low boundary layer heights in combination with a lack of knowledge of the tropospheric aerosol in the AMF calculation for the GEMS IUP-UB product. This is further discussed in Sect. 5.4.

During the summer months (JJA), the polluted stations (MAX-DOAS UB Incheon, Pandora Yonsei, Pandora Seoul) show a minimum in the $NO_2$ VCDs around 13 KST. Similar consistent results were found by Yang et al. (2024) and Edwards et al. (2024). This observation would fit the expectation that chemical loss is relatively rapid during noon, especially in summer, and significantly influences the diurnal variation of $NO_2$. However, this summer noon minimum is more pronounced in the stationary observations than in the GEMS IUP-UB columns, which show a smaller diurnal variation. Due to low data availability during the summer months in the GEMS L2 product after quality and cloud filtering, it is difficult to determine if this behavior is also present in the GEMS L2 observations.

Based on the reduced chemical loss of $NO_2$ during winter time and expected higher emissions, one would expect an accumulation of $NO_2$ and increasing tropospheric $NO_2$ VCDs over the day. This was also seen by Yang et al. (2024) for total column observations of GEMS, for the Pandora in Beijing, and the Pandora Seoul but not for Pandora Yonsei. However, this is not visible for the six sites analyzed here. On the contrary, the observed tropospheric $NO_2$ VCDs tend to decrease over the day. This is also visible for the GEMS L2 product in the Appendix Fig. A7.

The largest diurnal variation of tropospheric $NO_2$ VCDs are observed in spring and autumn. During these seasons, the polluted stations in the SMA show quite similar diurnal variation with increasing $NO_2$ in the morning, a maximum close to noon around 11/12 KST, and a decrease towards the evening. This agrees with previous studies, which found up to 40 % reduction of $NO_2$ columns in the OMI afternoon overpass compared to the SCIAMACHY morning over urban regions (Boersma et al., 2008, 2009) and similar reductions using GOME-2 morning and OMI afternoon observations over large urban regions in the US (Penn and Holloway, 2020). Also Edwards et al. (2024) showed that GEMS tropospheric $NO_2$ VCD variation can be large, especially in polluted environments (>50 % of the tropospheric VCD). However, the GEMS observations reveal that for the SMA the morning observations of SCIAMACHY and GOME-2 are in a period where tropospheric $NO_2$ is increasing, while the afternoon observations of OMI are in the period where the tropospheric NO2 VCD is decreasing, and the maximum of $NO_2$ in the SMA around noon is in between and not captured by previous missions.

If observations are averaged for a full year, the diurnal variation is distorted by the early and late data coming from the summer observations only because there are no scans in winter during these times. Deviations are largest in the early morning and late afternoon observations, which are for Korea available only from April to September. The diurnal variation of the median relative differences for the different seasons is shown in the Appendix Fig. A9. The diurnal variation of the deviations is similar over the seasons. However, the GEMS IUP-UB summer observations show a larger negative bias during summer. Due to the limited number of sites and observations available in summer, further investigation is needed The median relative differences at the individual sites are also summarized in a heatmap time series plot in the Appendix Fig. A8. In general, no overall sea-

sonality of the biases is visible. For the Pandora Seoul site, the discussed positive bias is visible for the autumn observations and needs to be further investigated.

### 5.2 Effects of wind speed and transport processes

Figure 7 and Fig. 8 illustrate the sensitivity of the diurnal variation of the tropospheric $NO_2$ VCDs to wind speed. Observations are separated into calm (wind speeds $< 3\,\mathrm{ms}^{-1}$, Fig. 7) and windy (wind speeds $\geq 3\,\mathrm{ms}^{-1}$, Fig. 8) conditions based on ERA5 10 m wind data (Hersbach et al., 2023), temporally and spatially interpolated to the GEMS observations. Due to reduced data availability after the separation, only selected sites are shown. The diurnal variation is quite different for calm and windy conditions for some of the shown sites and seasons but consistent for the GEMS IUP-UB and the ground-based data. However, the agreement is better for windy conditions than for low wind speeds, which can be explained by increased dispersion during windy conditions, resulting in fewer inhomogeneities. For calm conditions, the tropospheric $NO_2$ VCDs are generally larger due to the accumulation of local emissions (see also Chong et al. (2018)). For windy conditions, the observations show much less variation over the day because emissions are dispersed quickly. Differences between calm and windy conditions are smaller for the less polluted sites.

At the Busan site, the Pandora data show an increase of $NO_2$ during the afternoon in spring and summer for windy conditions (Fig. 8). Which is not captured by GEMS and is not visible during calm conditions. This increase might be explained by local

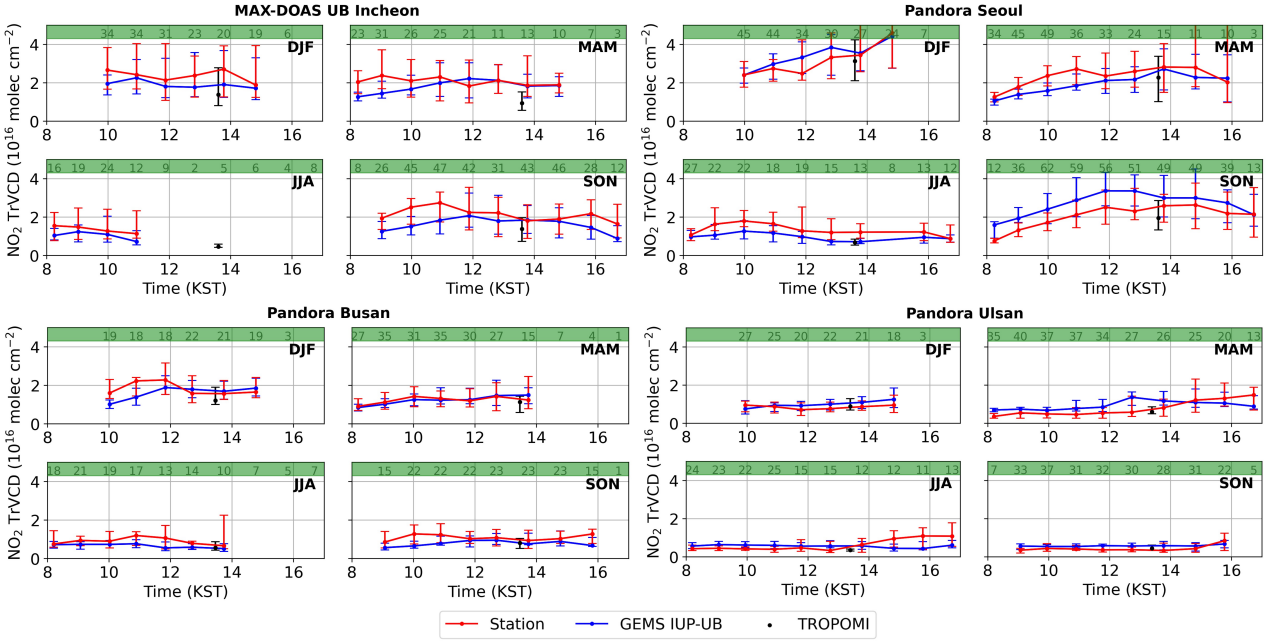


**Figure 7.** Same as Fig. 6 but only including tropospheric $NO_2$ VCDs with wind speeds $< 3\,\mathrm{ms}^{-1}$ for selected sites with still good data availability.

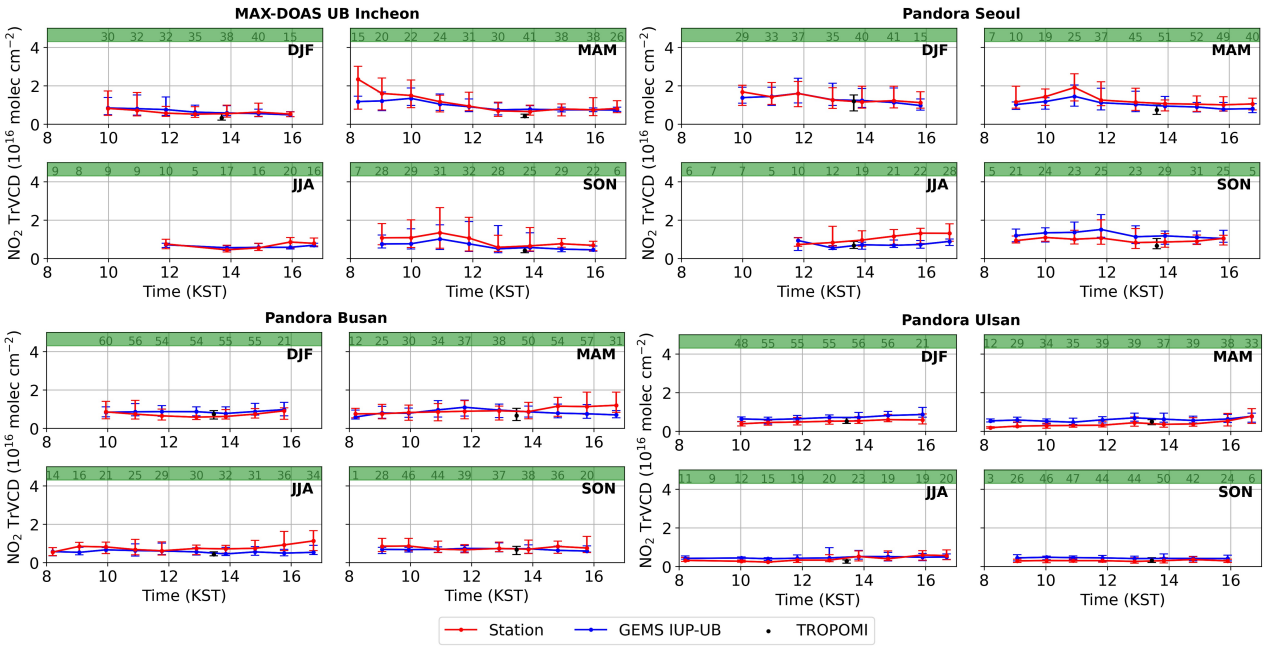


**Figure 8.** Same as Fig. 6 but only including tropospheric $NO_2$ VCDs with wind speeds $\geq 3\,\mathrm{ms}^{-1}$ for selected sites with still good data availability.

transport effects, which move $NO_2$ in the line of sight of the Pandora with the wind changing to southerly directions in the afternoon (see Fig. 9).

The largest differences between calm and windy conditions and between the seasons are found for the Pandora Seoul, the most polluted site of the four. During calm days in winter, the $NO_2$ shows a strong increase over the day. This can be attributed to the less effective chemical loss in winter and the accumulation of emissions that cannot be balanced by dilution on calm days. This increase over the day in winter was also shown based on GEMS total $NO_2$ columns by Yang et al. (2024). Yang et al. (2024) saw this increase already for all winter data without a wind filter, which is not visible in our tropospheric $NO_2$ VCD data set. After filtering only low wind conditions they observed an even stronger increase. For spring and autumn, the $NO_2$ increases in the morning, starts decreasing again around noon and flattens out in the afternoon. During summer, when the chemical loss is more effective, the minimum is around noon, but in general, there is less variation.

A significant increase is visible in the tropospheric $NO_2$ VCDs for the Pandora Ulsan site in spring during low wind speed conditions. Similar also during summer but then not captured by GEMS. The increase is not happening over the whole day but starting around noon, slightly later for the station data. This increase can be explained by transport effects, as illustrated by Fig. 9. Chong et al. (2018) observed similar transport effects for other remote Pandora sites close to emission sources during the Megacity Air Pollution Studies-Seoul (MAPS-Seoul) campaign from May to June 2015. This kind of transport effects can now be better followed and understood by the hourly maps of tropospheric $NO_2$ VCD observation provided by GEMS observations.

Figure 9 shows maps of GEMS IUP-UB tropospheric $NO_2$ VCDs averaged for May 2022 for each of the ten observations per day. Overlaid are the interpolated ERA5 10 m wind data. The maps show the southeast of South Korea, including the sites of the Pandora Busan, the MAX-DOAS MPIC Busan, the Pandora Ulsan, and the MAX-DOAS Ulsan. The GEMS IUP-UB

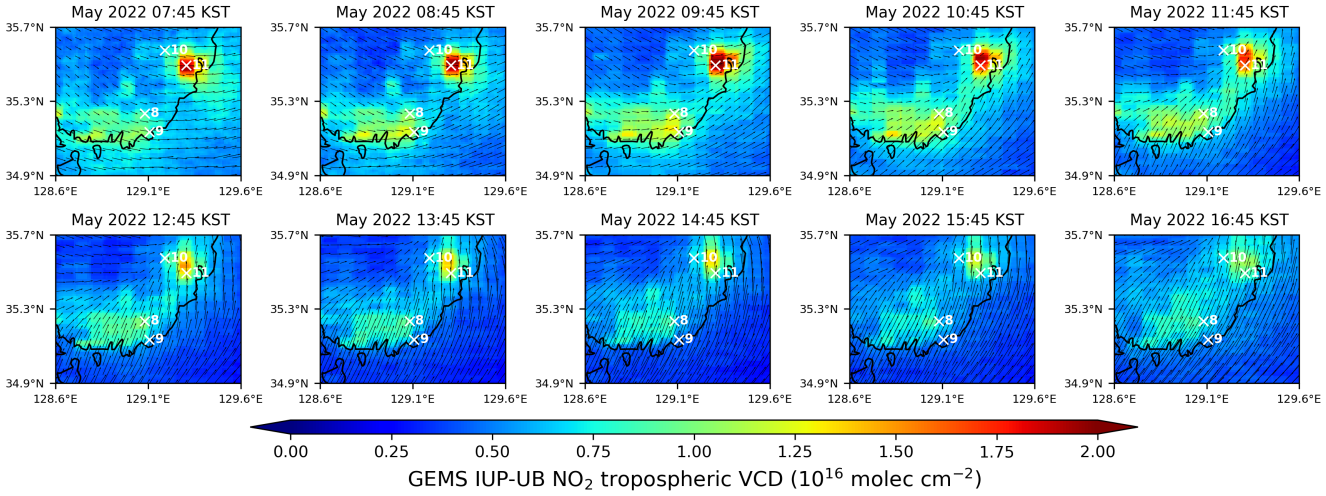


**Figure 9.** Maps of GEMS IUP-UB tropospheric $NO_2$ VCDs for the ten observations per day averaged for May 2022 overlaid with ERA5 10 m wind data. Arrow lengths indicate wind speed, and their orientation represents wind direction. Maps show the southeast of South Korea, including the sites of the Pandora Busan (8), the MAX-DOAS MPIC Busan (9), the Pandora Ulsan (10), and the MAX-DOAS Ulsan (11). Hourly monthly averaged maps for the SMA are shown in the Appendix Fig. A10

$NO_2$ columns are highest in the late morning observations and are decreasing towards the evening. The location of the $NO_2$ maximum varies over the day, clearly visible along the coastline and from its location relative to the station sites. In the early morning, the $NO_2$ is mainly located at the MAX-DOAS UB Ulsan site. With the wind turning from mainly westerly in the morning to mainly southerly winds around noon, the $NO_2$ is moving northwards. Therefore, the $NO_2$ is moving closer to the Pandora Ulsan site, which can explain the increase starting around noon visible in the spring diurnal variation plot. Hourly monthly averaged maps for the SMA showing the $NO_2$ build-up during the morning and transport over the day are shown in the Appendix Fig. A10.

In addition to the diurnal variation of transport effects due to changing wind direction, Fig. 10 illustrates the seasonal variability. Shown are maps of monthly averaged GEMS IUP-UB tropospheric $NO_2$ VCDs for the 13:45 KST observation from October 2021 to September 2022 for the southeast of South Korea, with overlaid ERA5 10 m wind data. The GEMS IUP-UB $NO_2$ columns are highest from late autumn to early spring and have their minimum during the summer months. From September to January, with a mainly northwesterly wind direction, a large part of the $NO_2$ is located over the ocean and mostly south of the ground-based stations. During spring, when the wind is changing from northwest to mostly southwest, the $NO_2$ is moving northwards.

The described influences of wind speed, causing dispersion or accumulation, and transport effects due to varying wind direc-

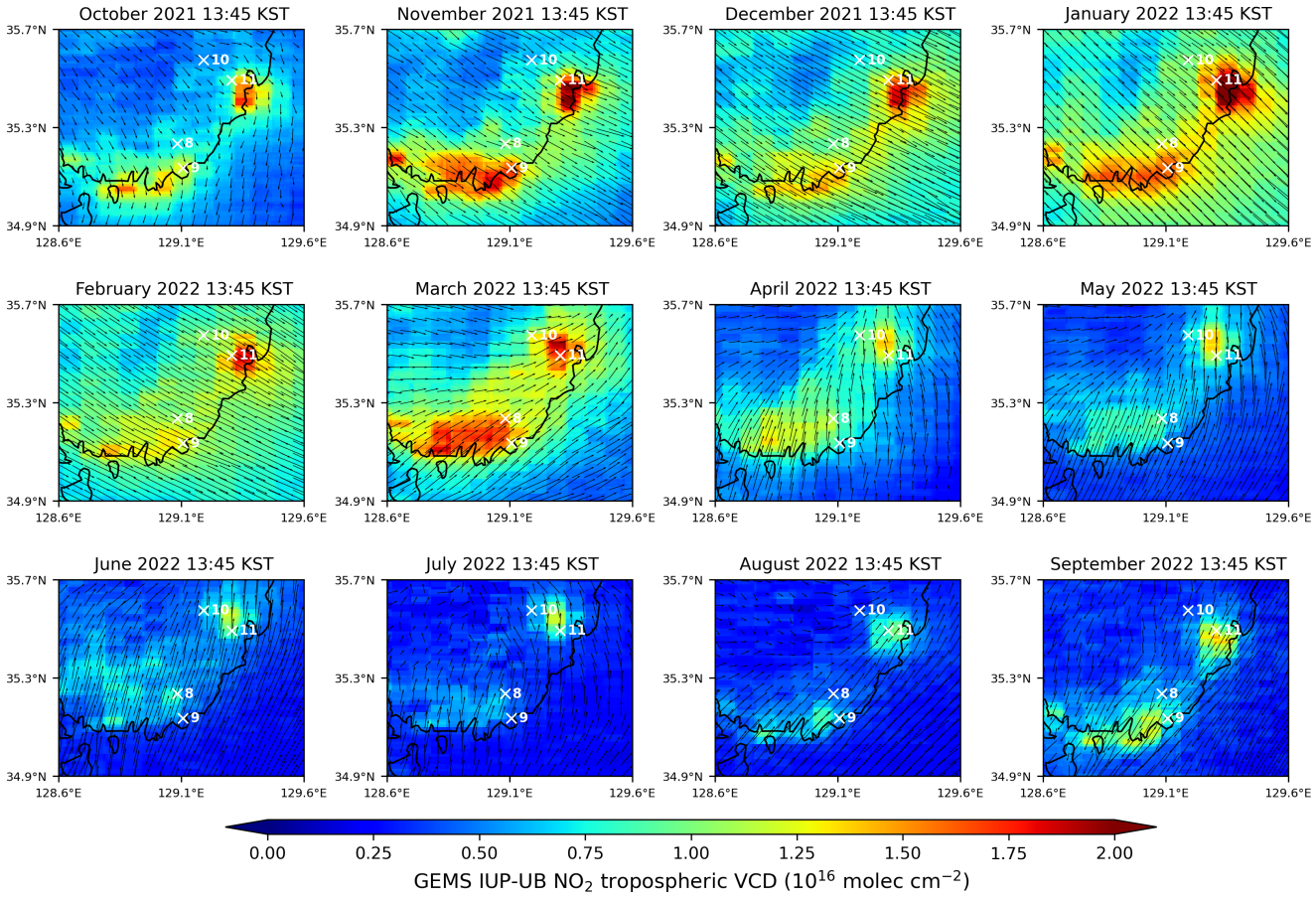


**Figure 10.** Maps of monthly averaged GEMS IUP-UB tropospheric $NO_2$ VCDs for the 13:45 KST observation from October 2021 to September 2022 overlaid with averaged ERA5 10 m wind data. Arrow lengths indicate wind speed, and their orientation represents wind direction. Maps show the southeast of South Korea, including the sites of the Pandora Busan (8), the MAX-DOAS MPIC Busan (9), the Pandora Ulsan (10), and the MAX-DOAS Ulsan (11).

tions over the day and the year, complicate the interpretation of observed diurnal variations of tropospheric $NO_2$ VCDs in terms of emissions and chemistry.

### 5.3 Weekday-weekend effect

480 Another influence on the diurnal variation of $NO_2$ is the difference in emissions on working days and those on weekends (Beirle et al., 2003; Stavrakou et al., 2020, e.g.,). Figure 11 shows the tropospheric $NO_2$ VCDs of the day of the week normalized with the mean $NO_2$ from Monday to Friday for the GEMS L2, the GEMS IUP-UB, and the TROPOMI observations with the collocated station observations. GEMS observations are averaged over all available observations per day. TROPOMI observations are only available once or twice a day in cloud-free conditions. Therefore, some deviations between the TROPOMI and GEMS

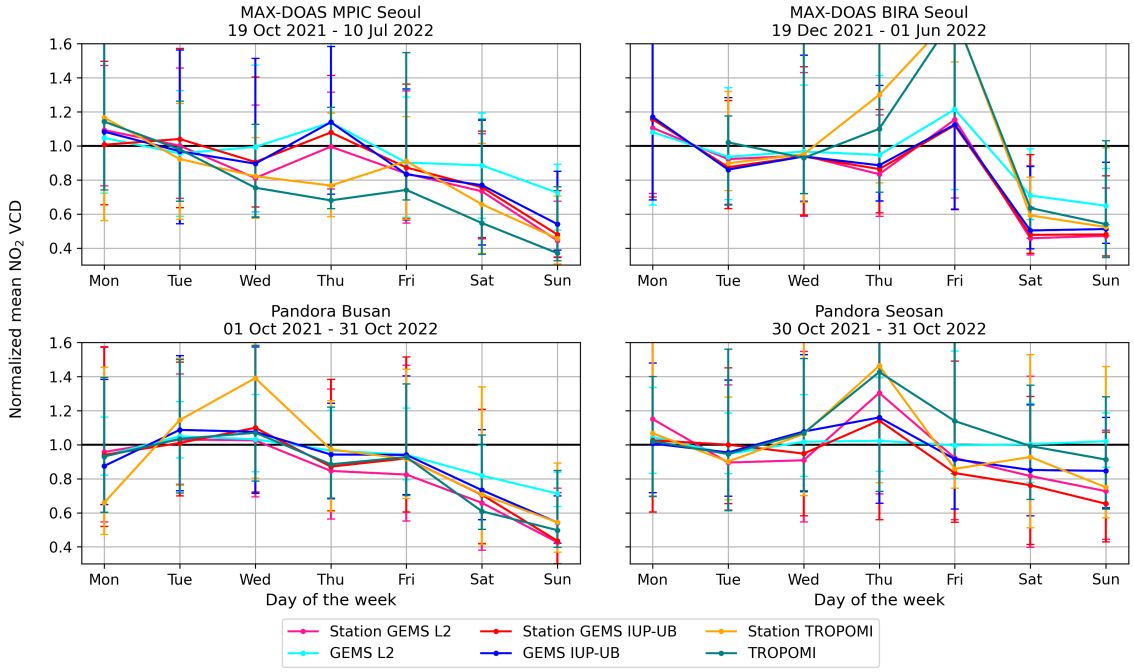


**Figure 11.** Plots of normalized weekday tropospheric $NO_2$ VCDs for co-located station observations with the the GEMS L2 (cyan), GEMS IUP-UB (blue), and the TROPOMI (turquoise) observations. The corresponding station measurements are marked in pink for the GEMS L2 product, in red for the GEMS IUP-UB product, and in yellow for the TROPOMI product. Station names and operation periods can be found in the individual titles. More sites are shown in the Appendix Fig. A11

tropospheric $NO_2$ VCD are explained by the reduced data availability and the timing effect. Due to different sampling of the three satellite products, each has its own coincident stationary data set.

Generally, there is a good agreement between the respective satellite products and their corresponding ground-based measurements. Similarly, there is good agreement among the different $NO_2$ products, with a few exceptions, mainly caused by the sparse TROPOMI observations. During the weekdays, from Monday to Friday, most normalized VCDs are close to one. Already on Saturday, the $NO_2$ is reduced compared to the weekdays. On Sundays, the $NO_2$ is reduced between around 20 % and 50 % compared to the average observed on weekdays. This reduction is significantly larger than the 10-20 % found in studies based on OMI and GOME data over Seoul (Beirle et al., 2003; Stavrakou et al., 2020). The smallest decline over the weekend is observed in Seosan, a more remote site with less influence from traffic emissions. MAX-DOAS BIRA Seoul and MAX-DOAS MPIC Seoul, both located in Seoul, still show some differences. $NO_2$ at the MAX-DOAS BIRA Seoul site peaks on Fridays and shows similarly strong reductions on Saturdays and Sundays, while at MAX-DOAS MPIC Seoul $NO_2$ peaks on Thursdays, and the reductions start Friday and are strongest on Sundays. This could be due to local differences but also to slightly different months in which the stations are operated and the data analyzed. Large differences in the TROPOMI observations compared to the GEMS observations, e.g., Fridays for the MAX-DOAS BIRA Seoul site, can be explained by the different sampling with

observations between 12:28 KST, and 14:37 KST, which might be biased to certain weeks or months because of cloud cover. The GEMS L2 product shows a distinct deviation on the weekend. The agreement with the other data sets is very good during the weekdays, but on Saturday and Sunday, there is less reduction compared to the average observed on weekdays than for the other products. One possible explanation is the in general higher background $NO_2$ values in the GEMS L2 product, which do not have a weekly cycle.

### 5.4 Discussion of GEMS - ground-based deviations

The agreement between the GEMS and the ground-based tropospheric $NO_2$ VCDs is promising. However, possible explanations for observed differences have to be discussed.

One potential reason for deviations between the GEMS and ground-based observations could be a poor stratospheric correction. Since the contribution of the stratosphere is small with column densities in the order of $10^{15}\,\mathrm{molec\,cm^{-2}}$, especially compared to the typically observed tropospheric $NO_2$ VCDs in the range of up to $1 \times 10^{17}\,\mathrm{molec\,cm^{-2}}$, the influence is not very large. However, under some conditions, the operational GEMS product has a large bias in the stratospheric columns, and in such situations, the stratospheric correction can be a significant source of error. To investigate the influence of the different stratospheric VCD products, subversions of the GEMS IUP-UB product, using different stratospheric column products, were created. Figure 12 shows scatter plots of coincident satellite and ground-based tropospheric $NO_2$ VCDs for (a) the original GEMS IUP-UB product using the STREAM-based stratospheric VCDs, (b) the GEMS IUP-UB using the TM5 stratospheric VCDs, (c) the GEMS IUP-UB using the GEMS L2 stratospheric VCDs, and (d) the original GEMS L2 product. Replacing the STREAM-based stratospheric VCDs with the TM5 stratospheric VCDs increases the bias from 3 % (-22 % - 38 %) to -20 % (-41 % - 5 %) and changes the offset from $+1.6 \times 10^{15}\,\mathrm{molec\,cm^{-2}}$ to $-3.9 \times 10^{14}\,\mathrm{molec\,cm^{-2}}$. This illustrates that the TM5 model stratospheric VCDs are too large, resulting in too low and even negative tropospheric $NO_2$ VCDs in the GEMS IUP-UB retrieval. Using the GEMS L2 stratospheric VCDs for the GEMS IUP-UB product, increases the bias and the offset, illustrating that the GEMS L2 stratospheric VCD product is too low. This results in an overestimation of the GEMS IUP-UB tropospheric $NO_2$ VCD compared to the station data. The correlation stays constant for both subversions as there is little correlation between the stratospheric $NO_2$ columns and the tropospheric $NO_2$ variations at the stations. The larger scatter in the operational GEMS L2 product is investigated in the following. The diurnal variation of the stratospheric $NO_2$ VCD products is shown in the Appendix Fig. A12. As expected, the TM5 model stratospheric VCDs, which are used for the TROPOMI product, agree well with the TROPOMI stratospheric $NO_2$ VCD value. The GEMS IUP-UB STREAM-based stratospheric columns show a very similar diurnal evolution as the TM5 data but are slightly lower. The GEMS L2 product shows a similar but slightly less variation over the day and is lower by a factor of around 2.5 when compared to the TM5 and GEMS IUP-UB stratospheric columns.

Another explanation for deviations between the GEMS and ground-based observations could be the effect of the Bidirectional Reflectance Distribution Function (BRDF), especially for the observations of diurnal evolution. However, the GEMS L2 product considers the BRDF influence using GEMS reflectivity data, yet the discrepancy with the ground-based data remains. To investigate the BRDF effect on the GEMS IUP-UB product, we replaced the TROPOMI LER product, used in the GEMS IUP-

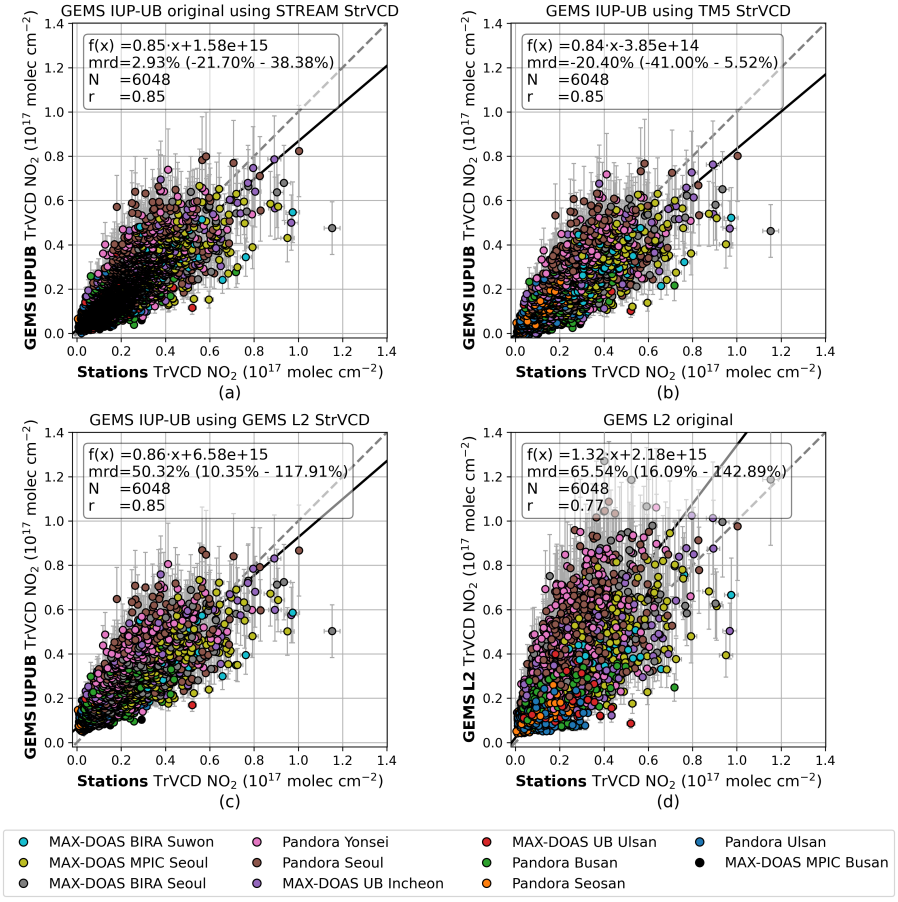


**Figure 12.** Scatter plots of satellite vs. co-located ground-based $NO_2$ tropospheric VCDs; for (a) the original GEMS IUP-UB product using the STREAM-based stratospheric VCDs, (b) the GEMS IUP-UB using the TM5 stratospheric VCDs, (c) the GEMS IUP-UB using the GEMS L2 stratospheric VCDs, and (d) the original GEMS L2 product.

UB product, with the GEMS L2 reflectivity. Figure 13 shows the scatter plots of (a) the GEMS L2 product using the GEMS L2 reflectivity in the AMF calculation, (b) the GEMS IUP-UB product using the TROPOMI LER reflectivity, both analyzed before, and (c) the modified GEMS IUP-UB product using the GEMS L2 reflectivity. The modified GEMS IUP-UB product shows more scatter than the original version and an overestimation similar to the GEMS L2 product, indicating that the GEMS reflectivity causes a large part of the overestimation and scatter.

Discrepancies between the MAX-DOAS and GEMS IUP-UB observations could be explained by the used model profiles. With its resolution of $1° \times 1°$, the TM5 model has a rather poor spatial resolution compared to the GEMS pixel size and the spatial variability of $NO_2$. Furthermore, it should be noted that the TM5 model has no specific focus on the GEMS region. Yang et al. (2023a) demonstrates that an updated version of the GEOS-Chem standard model with a resolution of $0.25° \times 0.3125°$ well reproduces diurnal variation of $NO_2$ vertical mixing observed during the KORUS-AQ campaign. This could be further

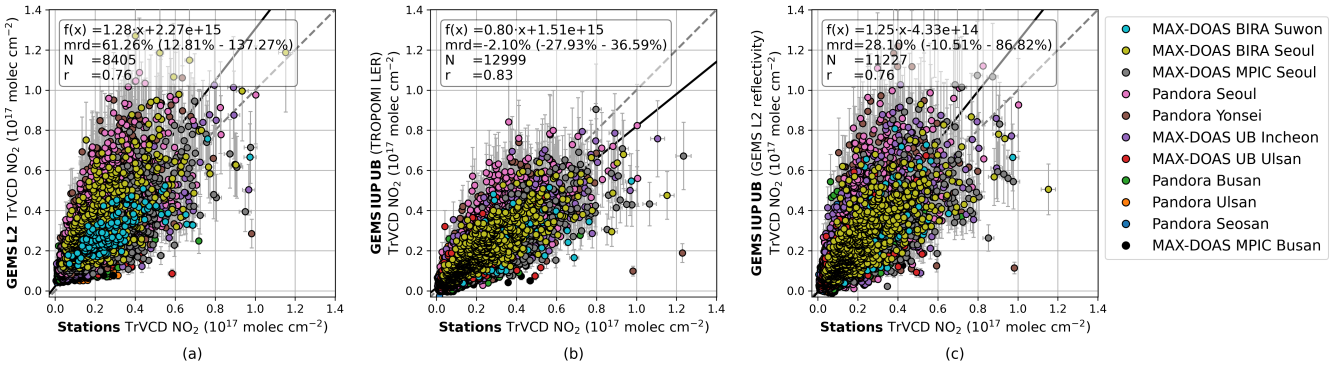


**Figure 13.** Scatter plots of satellite vs. co-located ground-based $NO_2$ tropospheric VCDs; for (a) the GEMS L2 product using the GEMS L2 reflectivity in the AMF calculation, (b) the GEMS IUP-UB product using the TROPOMI LER reflectivity, and (c) the GEMS IUP-UB product using the GEMS L2 reflectivity.

investigated by considering MAX-DOAS profiles and the GEMS averaging kernels. However, car DOAS measurements show that sometimes there can be large fluctuations within individual satellite pixels, and station measurements may be located in sub-pixel regions that are not representative of the entire pixel.

Another already mentioned aspect, which possibly contributes to the differences, especially at larger SZA, is the lack of knowledge of tropospheric aerosol in the calculation of the AMF for the GEMS IUP-UB product. However, the L2 product considers aerosol parameters from GEMS observations in the AMF determination and should be correct for their influence. The expected improvement is not reflected in the comparisons.

Due to less sensitivity at higher SZA (and VAA), AMFs are expected to be more uncertain for these scenes. This uncertainty is further enhanced for larger aerosol loads and with low boundary layer heights in the morning and evening.

## 6 Summary and conclusions

In this study we evaluated tropospheric $NO_2$ VCDs of the operational GEMS L2 v2.0, the scientific GEMS IUP-UB v1.0, and the operational TROPOMI v02.04.00 product with ground-based DOAS observations from 11 stationary and additional mobile car DOAS instruments in South Korea. GEMS is the first instrument in geostationary orbit, enabling the observation of diurnal variations of $NO_2$ over a large part of Asia. With its location centered over South Korea, GEMS provides up to 10 observations during daytime. The GEMS IUP-UB and the ground-based observations are used together with ERA5 10 m wind data to interpret the diurnal variation of tropospheric $NO_2$ VCDs.

Maps of tropospheric $NO_2$ VCDs from the GEMS L2, the GEMS IUP-UB, and the TROPOMI product, all around the the time of TROPOMI overpass, show the large $NO_2$ hot spots over the SMA and the smaller urban agglomerations. These hot spots, especially that above the SMA, show the highest values in the GEMS L2 product. The lowest values are found in the TROPOMI product. The background tropospheric $NO_2$ VCD is similar for the TROPOMI and the GEMS IUP-UB products

but is significantly higher in the GEMS L2 product, presumably because of the different approaches used for the stratospheric correction. Due to a missing interpolation of the AMF, the GEMS L2 product shows box structures with the spatial resolution of the GEOS-Chem model.

The evaluation of the GEMS L2 v2.0 tropospheric $NO_2$ VCD product with the ground-based DOAS measurements indicates an overestimation, with a slope of 1.28, a median relative difference of +61 %, and a correlation of 0.76. The evaluation results of the GEMS IUP-UB and the operational TROPOMI products show that both are low biased and have less scatter than the GEMS L2 product. The slope and median relative difference are 0.80 and -2 % for the GEMS IUP-UB product and 0.79 and -16 % for the TROPOMI product. The correlation of the GEMS products with the ground-based observations improves when observations are limited to the TROPOMI overpass time, indicating larger deviations in coinciding morning and/or afternoon observations. The separate comparison of the satellite and ground-based tropospheric $NO_2$ VCDs for the 11 individual sites illustrates some differences between the sites. Biases are larger for more polluted sites, while less polluted sites show differences closer to zero. The positive bias for the two least polluted sites is probably related to the stratospheric correction in the GEMS IUP-UB product. In general, the GEMS IUP-UB product and the TROPOMI product show good agreement in the individual biases. Mobile car DOAS observations serve as an additional data set to evaluate the GEMS observations and support the results obtained from the comparisons with stationary ground-based data.

Due to the locations of the stations in different pollution regimes, the observed diurnal variations of the tropospheric $NO_2$ VCDs from the GEMS IUP-UB and the ground-based data sets show different characteristics. Urban sites often show a maximum of $NO_2$ of varying degrees around 10/11 local time, while more rural sites show nearly no diurnal variation. For both cases, we find good agreement between the diurnal variation of the GEMS IUP-UB and the ground-based $NO_2$ data. The largest differences are visible in the morning and especially for the 16:45 KST observation, where the GEMS IUP-UB product often underestimates the station values. During summer the polluted sites show a minimum in the tropospheric $NO_2$ VCDs around noon (13 KST), indicating the larger influence of chemical loss in summer. However, this summer noon minimum is less pronounced in the GEMS observations than in the stationary observations. Winter observations show, in general, higher $NO_2$ values with rather flat or slightly decreasing $NO_2$ over the day, which is well captured in both data sets. We see no increase over the day, as reported by other studies using total $NO_2$ columns in Seoul and Beijing. Most diurnal variation is found at polluted sites in spring and autumn, with an increase during the morning, a maximum late in the morning or around noon, and a decrease towards the afternoon.

Diurnal variation differs significantly for low and high wind speed conditions in both the GEMS IUP-UB and the ground-based data set. However, there is better agreement during windy conditions, likely due to increased dispersion and reduced inhomogeneities. The influence of dispersion in windy conditions results in observations displaying less diurnal variation. Observations under low wind conditions show $NO_2$ increases over the day but only at the most polluted sites, especially during winter. This suggests that, under calm conditions, the reduced dilution and less effective chemical loss in winter are insufficient to offset the accumulating emissions. For a more rural site, the diurnal variation with increasing $NO_2$ values following mean wind patterns for specific seasons and times reveals the impact of transported $NO_2$. Due to a location-specific change in wind direction around noon, which is characteristic for these months, $NO_2$ pollution from an industrial area is transported close to

the station. This is also observed in other areas and on a seasonal basis.

When analyzing the weekday-weekend effect, a good agreement is found between the different tropospheric $NO_2$ VCD products. Dependent on the station, the $NO_2$ columns are 20 to 50 % lower on Sundays compared to the weekday average. However, the GEMS L2 product which agrees with the other data sets during weekdays shows significantly less reduction on weekends. Presumably caused by the generally higher $NO_2$ background values in the GEMS L2 product, which do not have a weekly cycle.

Significant impacts of both the stratospheric correction and the surface reflectivity on the GEMS tropospheric $NO_2$ VCD products were found. While the GEMS L2 stratospheric VCD is too low, resulting in too high tropospheric $NO_2$ VCDs, the TM5 model's stratospheric VCDs, used in the TROPOMI product, are too high, resulting in too low tropospheric $NO_2$ VCDs, when implemented in the GEMS IUP-UB retrieval. Surface reflectivity comparisons indicate that the GEMS L2 reflectivity is a major contributor to the observed overestimation and scattering in the GEMS tropospheric $NO_2$ VCD product.

Deviations between GEMS and ground-based observations at larger SZA might be explainable by a lower sensitivity and more uncertain AMFs for these scenes, which is amplified for larger aerosol loads and low boundary layer heights in combination with a lack of knowledge of the tropospheric aerosol in the AMF calculation for the GEMS IUP-UB product. This shows the increasing importance to have good aerosol information and to include them in the AMF calculations.

Overall, our analyses revealed significant diurnal variation of $NO_2$. This variation is strongly site-dependent, differs between polluted and less polluted sites, and has location-specific and seasonal characteristics. GEMS IUP-UB and ground-based observations are in good agreement. This is promising for the extension of the analysis of diurnal variation of tropospheric $NO_2$ using the extensive GEMS data set in other parts of Asia. The observed diurnal variation of $NO_2$ offers unique insights into the chemistry and emission of $NO_x$ as well as transport processes, but it needs to be carefully interpreted. Our analysis shows significant impacts of both the stratospheric correction and the surface reflectivity data on the GEMS tropospheric $NO_2$ VCD products. These analyses can also help to analyze the upcoming data sets of the follow-up geostationary air quality missions such as TEMPO over North America and Sentinel-4 over Europe.

*Data availability.* GEMS L2 $NO_2$ data can be accessed at https://nesc.nier.go.kr/en/html/cntnts/91/static/page.do (National Institute of Environmental Research, NIER, 2023). The GEMS IUP-UB $NO_2$ product is available on request. TROPOMI $NO_2$ data are freely available via https://s5phub.copernicus.eu/ (Sentinel-5P Pre-Operations Data Hub, last access: 21 February 2022). The data of Pandora instruments are freely available from the PGN data archive (https://pandonia-global-network.org/, last access: 11 October 2023). The FRM4DOAS MAX-DOAS data are available on request. The ERA5 wind data are freely available from the Copernicus Climate Change (C3S) climate data store (CDS) (Hersbach et al., 2023).

*Author contributions.* All co-authors contributed to the campaign either as participants and instrument operators and/or during campaign preparation. AR provided the GEMS IUP-UB $NO_2$ data product. HL and HH provided information to the GEMS L2 $NO_2$ data product. CF and MMF performed the MAX-DOAS data analysis. The campaign was prepared by HH, LSC, and CKS. KL performed the final data analysis and interpreted the results together with AR. KL wrote the paper with feedback and contributions from all other co-authors.

*Competing interests.* At least one of the (co-)authors is a member of the editorial board of Atmospheric Measurement Techniques.

*Acknowledgements.* We thank the National Institute of Environmental Research of South Korea for providing GEMS data, financial support (NIER-2022-04-02-037), and the excellent organization of the GMAP 2021 and SIJAQ 2022 field campaigns. We thank all participants of the GMAP 2021 and SIJAQ 2022 field campaigns. The Deutsches Zentrum für Luft- und Raumfahrt (grant no. 50 EE 2204) is acknowledged for financial support. Copernicus Sentinel-5P level-2 $NO_2$ data are used in this study. Sentinel-5 Precursor is a European Space Agency (ESA) mission on behalf of the European Commission (EC). The TROPOMI payload is a joint development by ESA and the Netherlands Space Office (NSO). The Sentinel-5 Precursor ground-segment development has been funded by the ESA and with national contributions from the Netherlands, Germany, Belgium, and the UK. We thank PGN instrument PIs, support staff and funding for establishing and maintaining the Pandora sites used in this investigation. The PGN is a bilateral project supported with funding from NASA and ESA. MMF thanks R. Spurr for the free use of VLIDORT.

## Appendix A

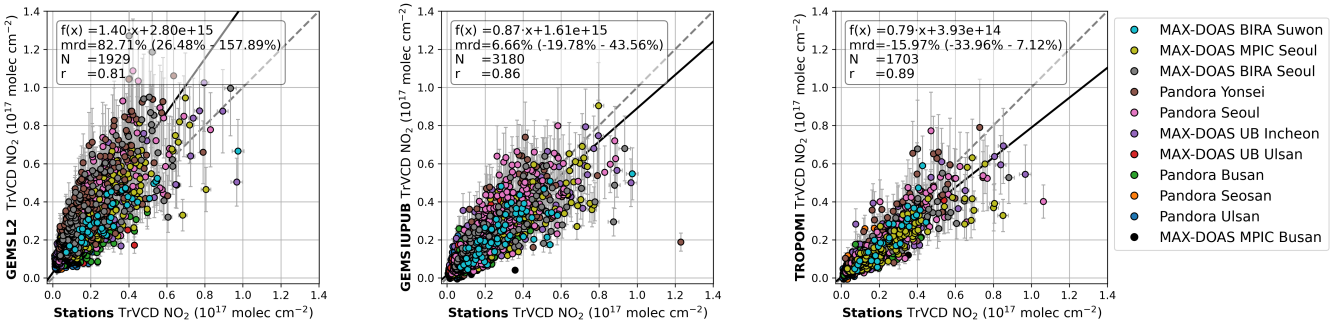


**Figure A1.** Same as Fig. 3 but GEMS L2 and GEMS IUP-UB observations are limited to the TROPOMI overpass time between 12:28 KST and 14:37 KST.

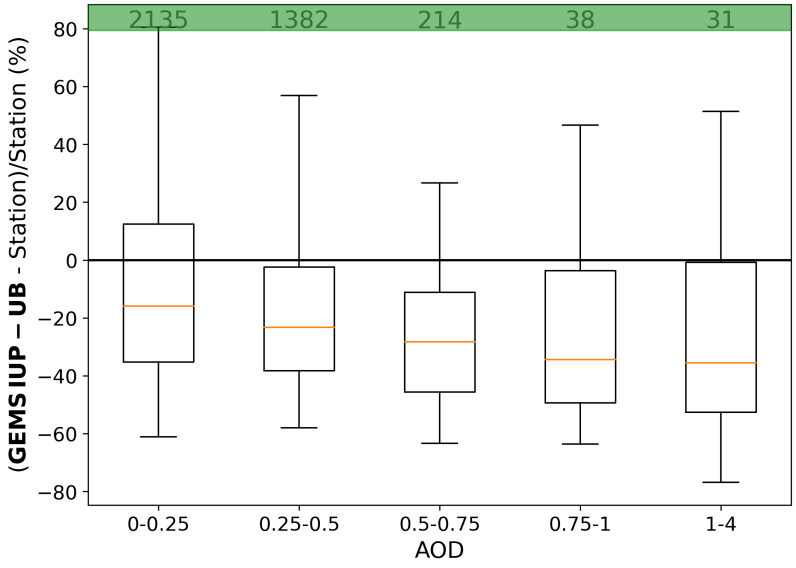


**Figure A2.** Median relative differences between GEMS IUP-UB and MAX-DOAS tropospheric $NO_2$ columns as a function of AOD retrieved within the FRM4DOAS MAX-DOAS $NO_2$ analysis. Numbers in the green bar represent the number of observations contributed to the bin.

The comparison of satellite and ground-based observations was investigated for different spatial co-location criteria: the closest pixels within a radius of 5 km respectively 10 km around the station sites, and considering the ground-based instruments viewing azimuth angle (VAA) during satellite overpass. To investigate the VAA dependence, the GEMS pixels $\mathrm{VCD_{sat}}$ are weighted according to their contribution along the line of sight $d$ of the ground-based instruments.

$$\mathrm{VCD_{sat,\,VAA}} = \frac{\sum \mathrm{VCD_{sat}}_{\,i} \cdot d_i}{\sum d_i} \tag{A1}$$

We consider the line of sight within 5 km to the station site. The comparison is only included in the analysis when more than 75 % of the line of sight is covered by satellite pixels. Measurements taken in the same VAA within the $\pm$20 min of the satellite observation, overlapping with the same GEMS pixels are averaged.

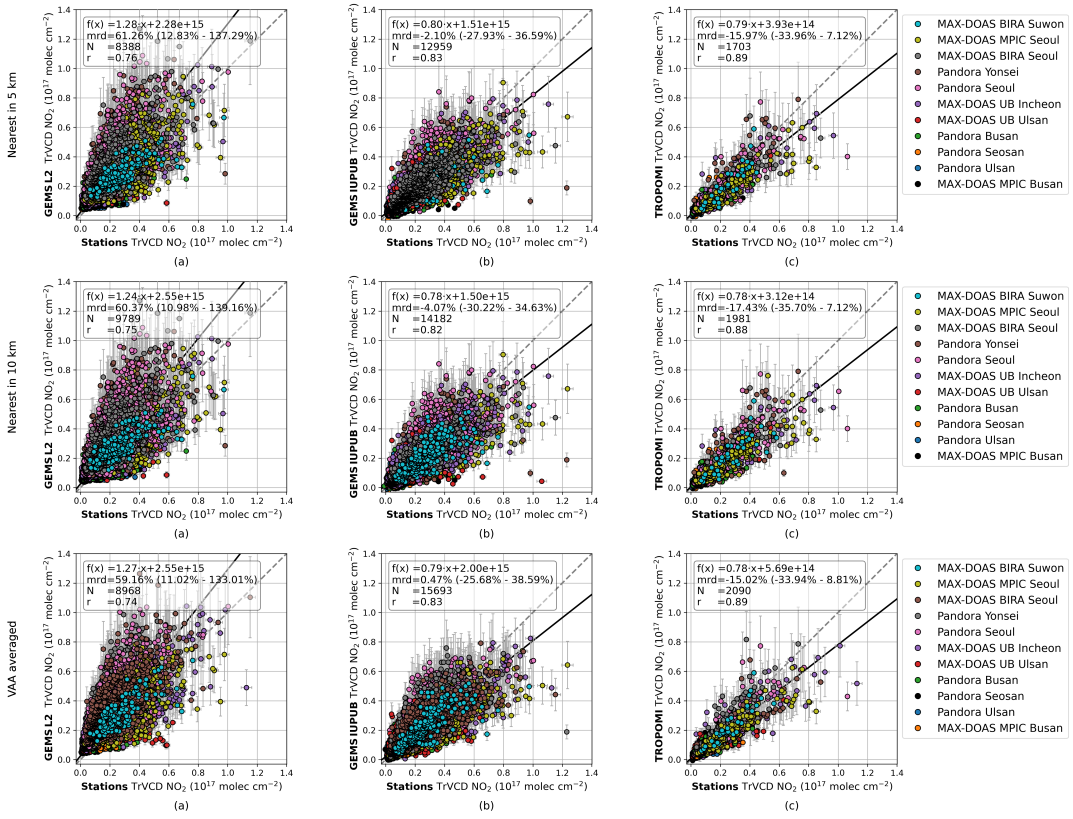


**Figure A3.** Scatter plots of GEMS L2 (a), GEMS IUP-UB (b), and TROPOMI (c) $NO_2$ tropospheric VCDs vs. co-located ground-based $NO_2$ tropospheric VCDs for different co-location criteria. The time constraint is $\pm$ 20 min around the time of the satellite measurement. First row: Ground-based measurements within this period are averaged and matched to the closest satellite observation within 5 km around the station site. Second row: Match to the closest satellite observation within 10 km. Third row: Satellite pixels are weighted according to their contribution along the line of sight of the ground-based instruments within 5 km of the station.

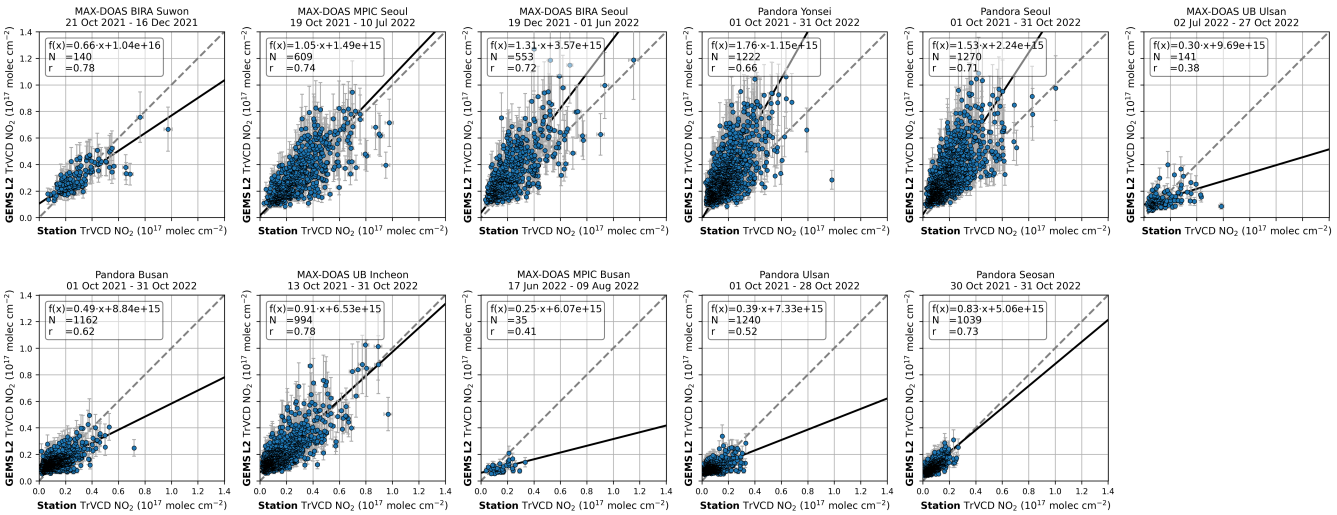


**Figure A4.** Scatter plots of GEMS L2 tropospheric $NO_2$ VCDs vs. co-located ground-based $NO_2$ tropospheric VCDs for the 11 individual sites. Station names and measurement periods can be found in the title. Co-location criteria are with $\pm$ 20 min and nearest 5 km the same as in Fig. 3.

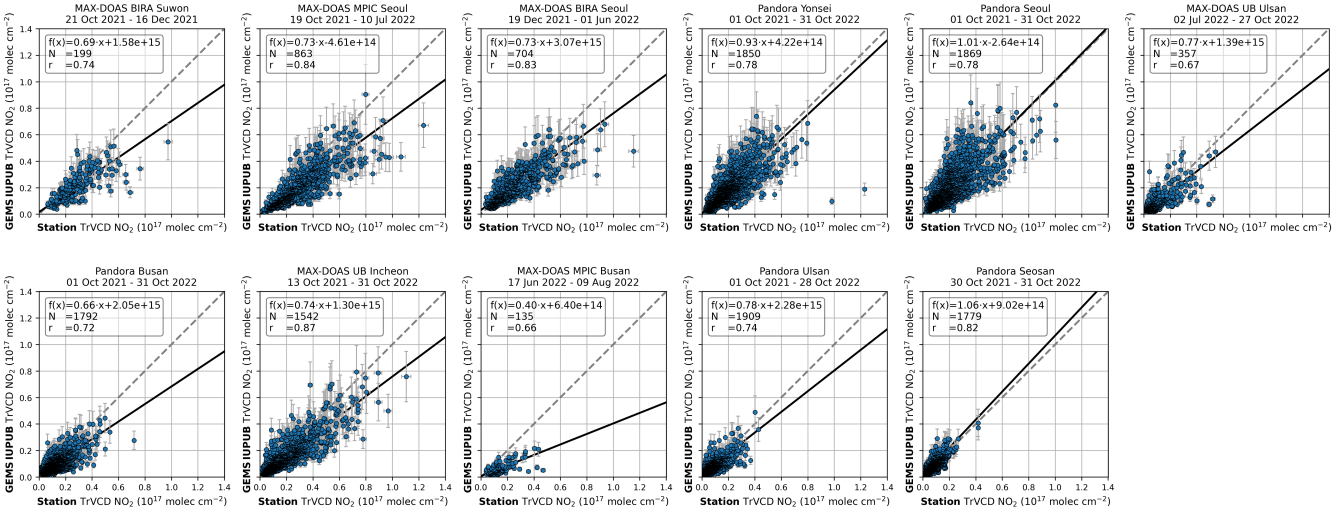


**Figure A5.** Same as Fig. A4 but for GEMS IUP-UB tropospheric $NO_2$ VCDs vs. co-located ground-based $NO_2$ tropospheric VCDs.

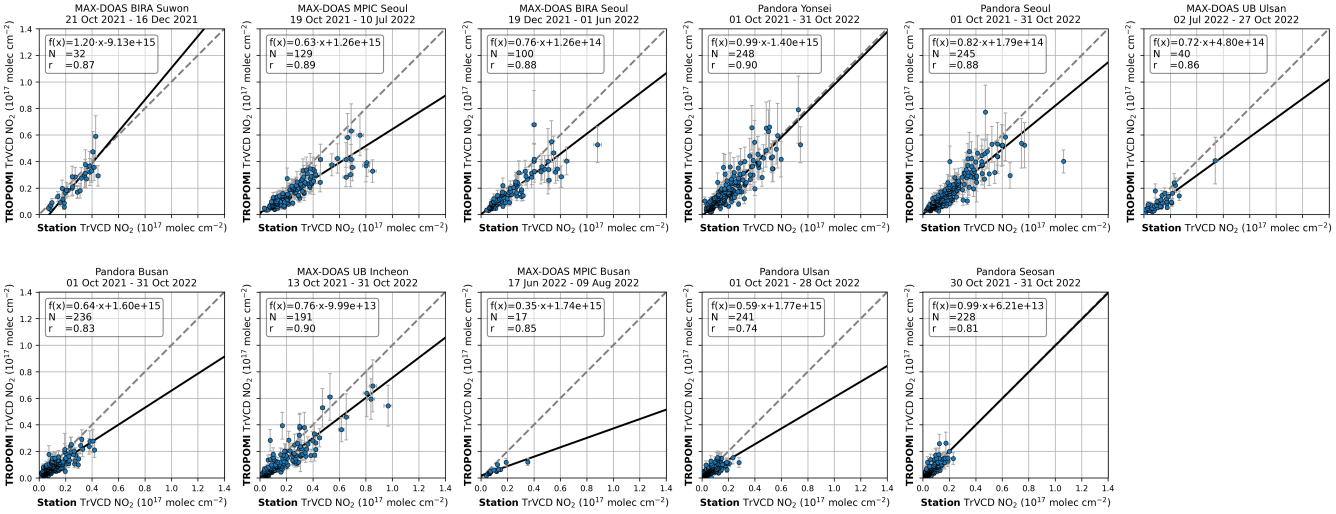


**Figure A6.** Same as Fig. A4 and A5 but for TROPOMI tropospheric $NO_2$ VCDs vs. co-located ground-based $NO_2$ tropospheric VCDs.

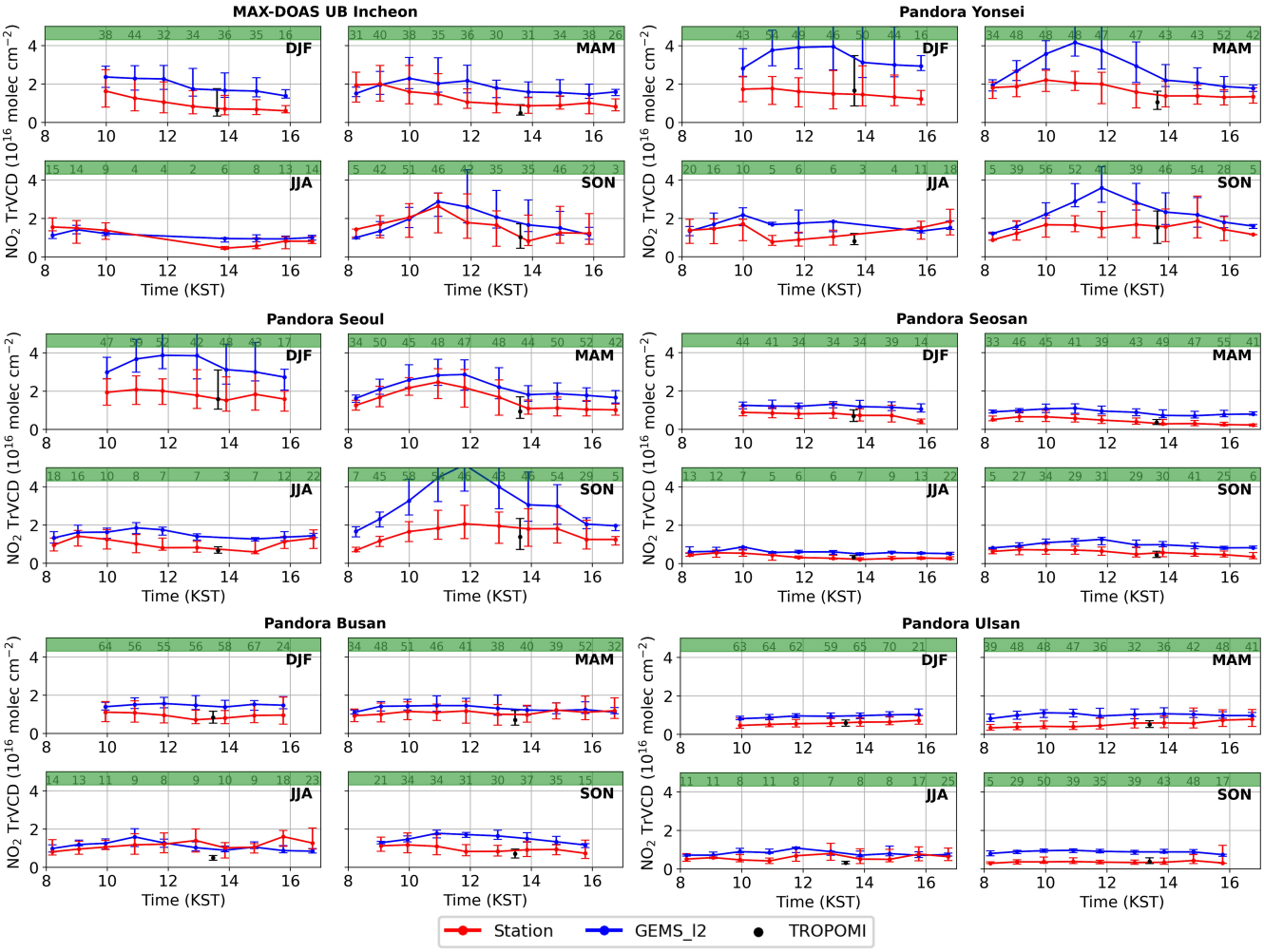


**Figure A7.** Same as Fig. 6 but for GEMS L2. Diurnal variation of median tropospheric $NO_2$ VCDs from the GEMS L2 product (blue) and ground-based stations (red) for the individual seasons (DJF, MAM, JJA, SON). The TROPOMI observation is added in black. Station names can be found in the individual titles. Vertical bars represent the 25 and 75 % quantiles of the MAX-DOAS and GEMS observations. Due to low data availability for the GEMS L2 product in summer, observations are displayed starting at five instead of 10 available observations, see green bar.

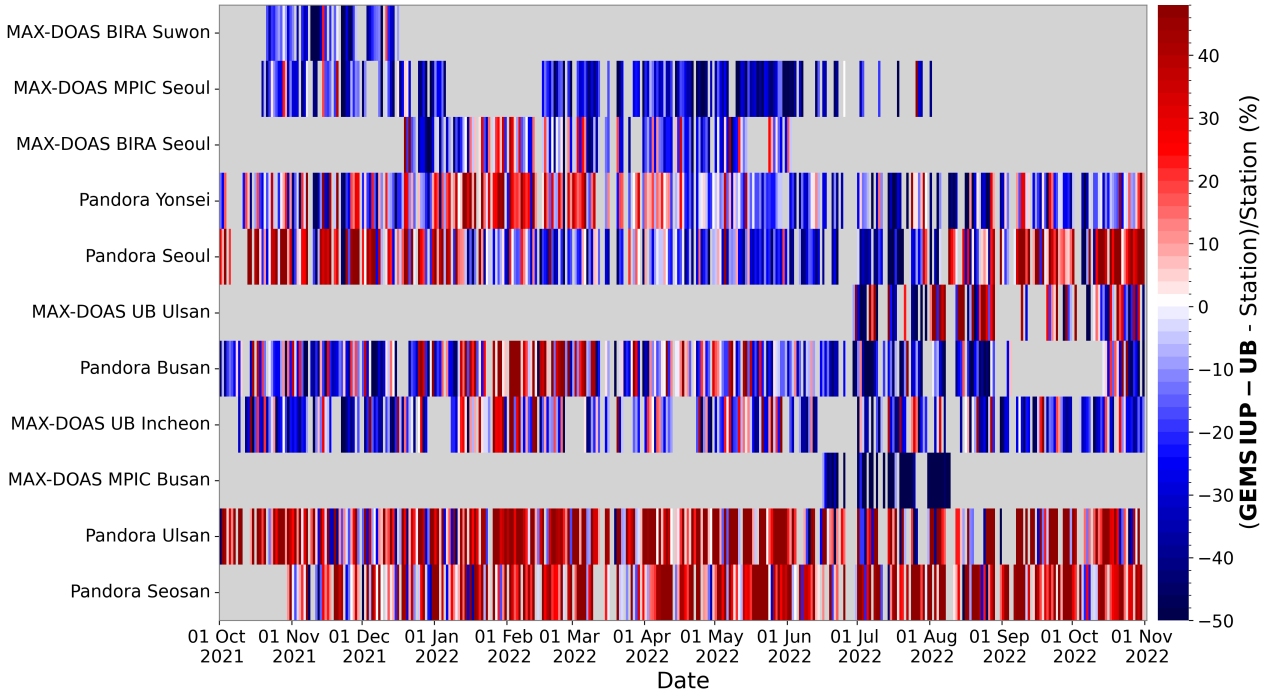


**Figure A8.** Time series of the median relative differences at the different ground-based sites from 1 October 2021 to 31 October 2022. The stations are ordered from bottom to top by increasing median ground-based tropospheric VCD.

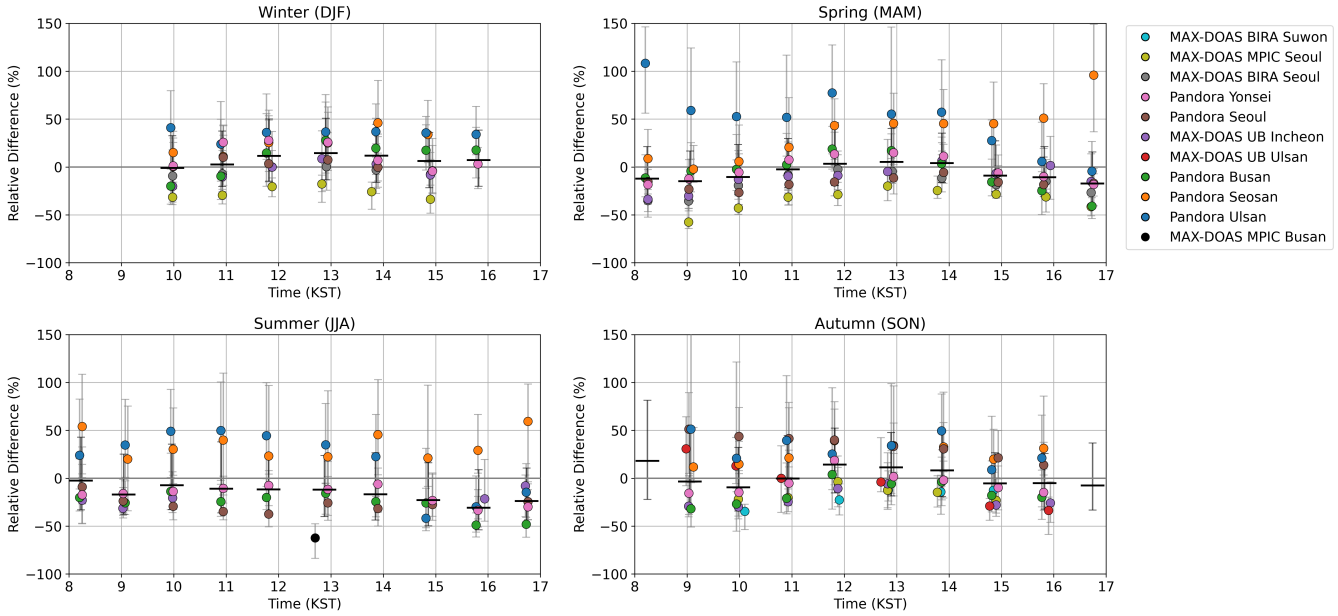


**Figure A9.** Diurnal variation of the median relative differences of the GEMS IUP-UB $NO_2$ product at the individual ground-based sites for the different seasons. Stations are color-coded. The median, including differences of all stations, is shown as black bars. Error bars represent the 25 and 75 % quantiles. Results are only included if more than 20 observations are available per time bin and station.

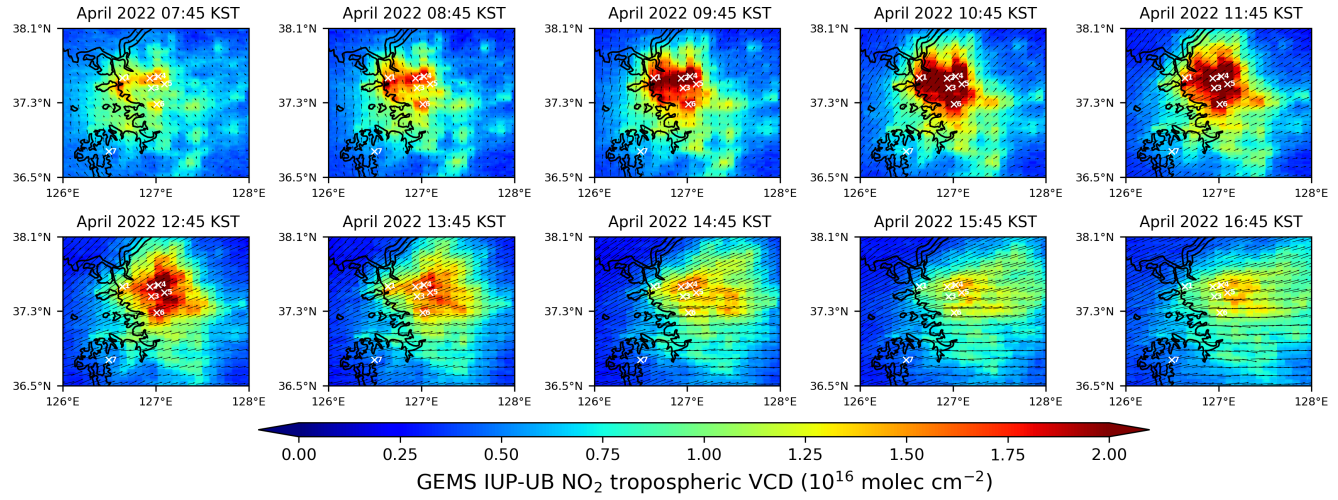


**Figure A10.** Maps of GEMS IUP-UB tropospheric $NO_2$ VCDs for the ten observations per day averaged for April 2022 overlaid with ERA5 10 m wind data. Arrow lengths indicate wind speed, and their orientation represents wind direction. Maps show the SMA, including the sites of the MAX-DOAS IUP-UB Incheon (1), Pandora Yonsei (2), Pandora Seoul (3), MAX-DOAS BIRA Seoul (4), MAX-DOAS MPIC Seoul (5), MAX-DOAS BIRA Suwon (6), and Pandora Seosan (7).

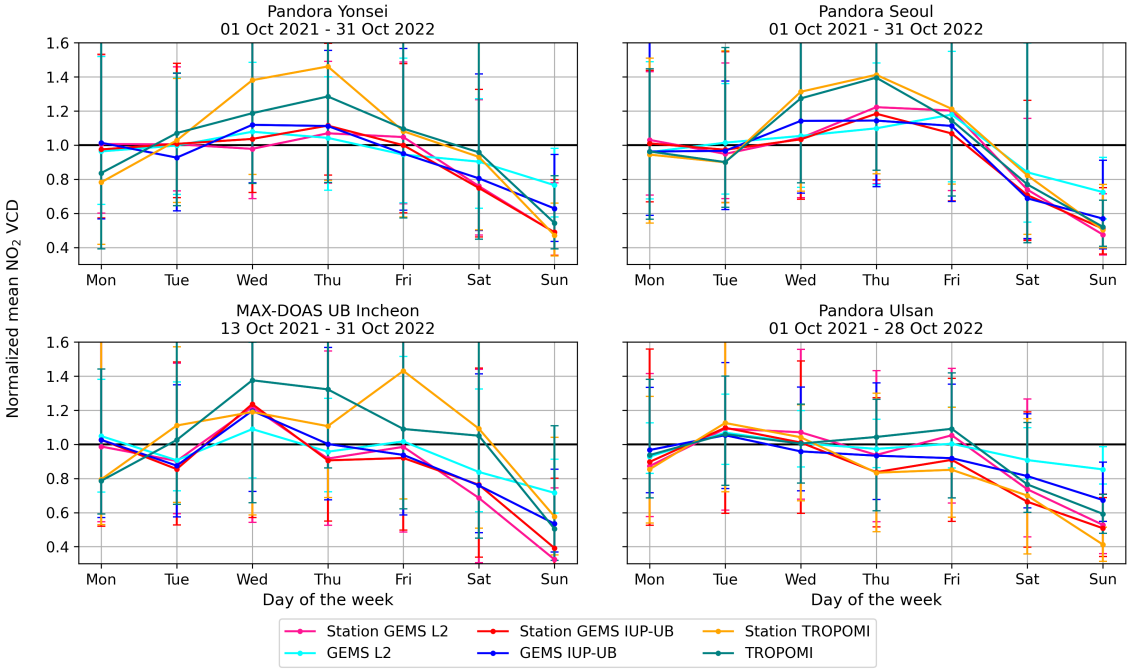


**Figure A11.** Remaining sites not shown in Fig. 11. Plots of normalized weekday $NO_2$ VCDs for the co-located station observations with the GEMS IUP-UB, the GEMS L2, and the TROPOMI observations.

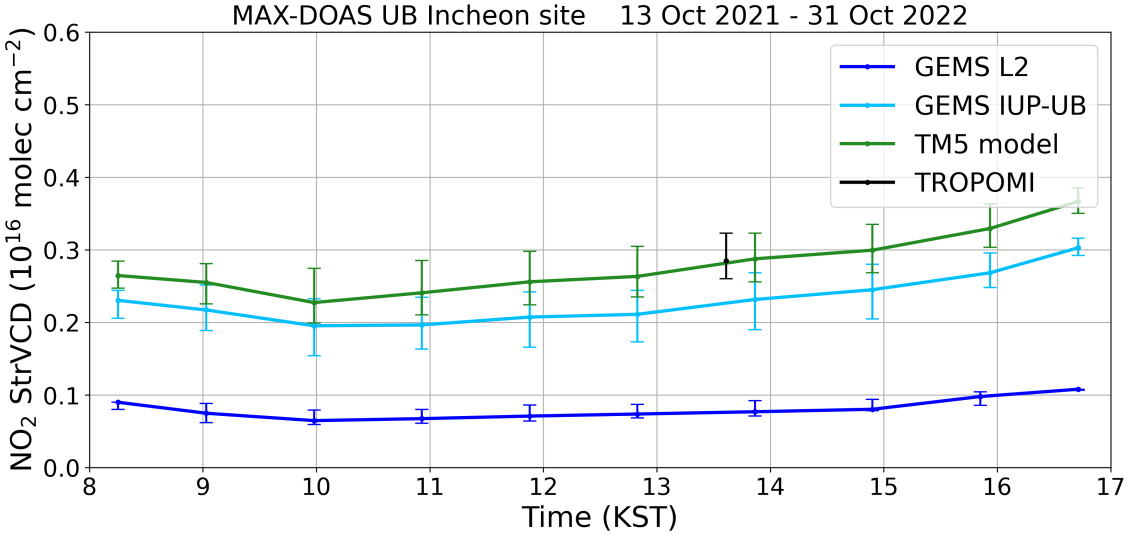


**Figure A12.** Diurnal variation of median stratospheric $NO_2$ VCDs for the GEMS L2 product based on the method from Bucsela et al. (2013) in dark blue, the GEMS IUP-UB STREAM-based product in light blue, and in green the TM5 model stratospheric VCDs, used for the TROPOMI product, which is shown in black.

## References


Beirle, S., Platt, U., Wenig, M., and Wagner, T.: Weekly cycle of $NO_2$ by GOME measurements: a signature of anthropogenic sources, Atmospheric Chemistry and Physics, 3, 2225–2232, https://doi.org/10.5194/acp-3-2225-2003, 2003.

Beirle, S., Boersma, K. F., Platt, U., Lawrence, M. G., and Wagner, T.: Megacity emissions and lifetimes of nitrogen oxides probed from space, Science, 333, 1737–1739, https://doi.org/10.1126/science.1207824, 2011.

Beirle, S., Hörmann, C., Jöckel, P., Liu, S., Penning de Vries, M., Pozzer, A., Sihler, H., Valks, P., and Wagner, T.: The STRatospheric Estimation Algorithm from Mainz (STREAM): estimating stratospheric $NO_2$ from nadir-viewing satellites by weighted convolution, Atmospheric Measurement Techniques, 9, 2753–2779, https://doi.org/10.5194/amt-9-2753-2016, 2016.

Beirle, S., Borger, C., Dörner, S., Li, A., Hu, Z., Liu, F., Wang, Y., and Wagner, T.: Pinpointing nitrogen oxide emissions from space, Science advances, 5, eaax9800, https://doi.org/10.1126/sciadv.aax9800, 2019a.

Beirle, S., Dörner, S., Donner, S., Remmers, J., Wang, Y., and Wagner, T.: The Mainz profile algorithm (MAPA), Atmospheric Measurement Techniques, 12, 1785–1806, https://doi.org/10.5194/amt-12-1785-2019, 2019b.

Boersma, K. F., Jacob, D. J., Eskes, H. J., Pinder, R. W., Wang, J., and van der A, R. J.: Intercomparison of SCIAMACHY and OMI tropospheric NO2 columns: Observing the diurnal evolution of chemistry and emissions from space, Journal of Geophysical Research: Atmospheres, 113, https://doi.org/10.1029/2007jd008816, 2008.

Boersma, K. F., Jacob, D. J., Trainic, M., Rudich, Y., DeSmedt, I., Dirksen, R., and Eskes, H. J.: Validation of urban NO2 concentrations and their diurnal and seasonal variations observed from the SCIAMACHY and OMI sensors using in situ surface measurements in Israeli cities, Atmospheric Chemistry and Physics, 9, 3867–3879, https://doi.org/10.5194/acp-9-3867-2009, 2009.

Bovensmann, H., Burrows, J., Buchwitz, M., Frerick, J., Noël, S., Rozanov, V., Chance, K., and Goede, A.: SCIAMACHY: Mission objectives and measurement modes, Journal of the atmospheric sciences, 56, 127–150, 1999.

Bucsela, E. J., Krotkov, N. A., Celarier, E. A., Lamsal, L. N., Swartz, W. H., Bhartia, P. K., Boersma, K. F., Veefkind, J. P., Gleason, J. F., and Pickering, K. E.: A new stratospheric and tropospheric $NO_2$ retrieval algorithm for nadir-viewing satellite instruments: applications to OMI, Atmospheric Measurement Techniques, 6, 2607–2626, https://doi.org/10.5194/amt-6-2607-2013, 2013.

Burrows, J., Bovensmann, H., Bergametti, G., Flaud, J., Orphal, J., Noël, S., Monks, P., Corlett, G., Goede, A., von Clarmann, T., Steck, T., Fischer, H., and Friedl-Vallon, F.: The geostationary tropospheric pollution explorer (GeoTROPE) mission: objectives, requirements and mission concept, Advances in Space Research, 34, 682–687, https://doi.org/10.1016/j.asr.2003.08.067, 2004.

Burrows, J. P., Weber, M., Buchwitz, M., Rozanov, V., Ladstätter-Weißenmayer, A., Richter, A., DeBeek, R., Hoogen, R., Bramstedt, K., Eichmann, K.-U., Eisinger, M., and Perner, D.: The Global Ozone Monitoring Experiment (GOME): Mission Concept and First Scientific Results, Journal of the Atmospheric Sciences, 56, 151 – 175, https://journals.ametsoc.org/view/journals/atsc/56/2/1520-0469_1999_056_0151_tgomeg_2.0.co_2.xml, 1999.

Cede, A.: Manual for Blick Software Suite 1.8, Tech. rep., last access: 24 January 2024, 2021.

Chong, H., Lee, H., Koo, J.-H., Kim, J., Jeong, U., Kim, W., Kim, S.-W., Herman, J. R., Abuhassan, N. K., Ahn, J.-Y., Park, J.-H., Kim, S.-K., Moon, K.-J., Choi, W.-J., and Park, S. S.: Regional Characteristics of NO2 Column Densities from Pandora Observations during the MAPS-Seoul Campaign, Aerosol and Air Quality Research, 18, 2207–2219, https://doi.org/10.4209/aaqr.2017.09.0341, 2018.

Dimitropoulou, E., Hendrick, F., Pinardi, G., Friedrich, M. M., Merlaud, A., Tack, F., De Longueville, H., Fayt, C., Hermans, C., Laffineur, Q., Fierens, F., and Van Roozendael, M.: Validation of TROPOMI tropospheric $NO_2$ columns using dual-scan multi-axis differential

optical absorption spectroscopy (MAX-DOAS) measurements in Uccle, Brussels, Atmospheric Measurement Techniques, 13, 5165–5191, https://doi.org/10.5194/amt-13-5165-2020, 2020.

Edwards, D. P., Martínez-Alonso, S., Jo, D. S., Ortega, I., Emmons, L. K., Orlando, J. J., Worden, H. M., Kim, J., Lee, H., Park, J., and Hong, H.: Quantifying the diurnal variation in atmospheric $NO_2$ from Geostationary Environment Monitoring Spectrometer (GEMS) observations, Atmospheric Chemistry and Physics, 24, 8943–8961, https://doi.org/10.5194/acp-24-8943-2024, 2024.

Eskes, H. and Eichmann, K.: S5P MPC Product Readme Nitrogen Dioxide, Tech. rep., last access: 14 December 2023, 2023.

Faustini, A., Rapp, R., and Forastiere, F.: Nitrogen dioxide and mortality: review and meta-analysis of long-term studies, European Respiratory Journal, 44, 744–753, https://doi.org/10.1183/09031936.00114713, 2014.

Friedrich, M. M., Rivera, C., Stremme, W., Ojeda, Z., Arellano, J., Bezanilla, A., García-Reynoso, J. A., and Grutter, M.: $NO_2$ vertical profiles and column densities from MAX-DOAS measurements in Mexico City, Atmospheric Measurement Techniques, 12, 2545–2565, https://doi.org/10.5194/amt-12-2545-2019, 2019.

Hendrick, F., Pinardi, G., Van Roozendael, M., Apituley, A., Piters, A., Richter, A., Wagner, T., Kreher, K., Friess, U., and Lampel, J.: Fiducial Reference Measurements for Ground-Based DOAS Air-Quality Observations, Deliverable D13 ESA Contract No.4000118181/16/I-EF, https://frm4doas.aeronomie.be/ProjectDir/Deliverables/FRM4DOAS_D13_Campaign_Planning_Document_20161021_final.pdf, last access 14 July 2022, 2016.

Herman, J., Cede, A., Spinei, E., Mount, G., Tzortziou, M., and Abuhassan, N.: NO2 column amounts from ground-based Pandora and MFDOAS spectrometers using the direct-sun DOAS technique: Intercomparisons and application to OMI validation, Journal of Geophysical Research: Atmospheres, 114, https://doi.org/10.1029/2009jd011848, 2009.

Hersbach, H., Bell, B., Berrisford, P., Biavati, G., Horányi, A., Muñoz Sabater, J., Nicolas, J., Peubey, C., Radu, R., Rozum, I., Schepers, D., Simmons, A., Soci, C., Dee, D., and Thépaut, J.-N.: ERA5 hourly data on single levels from 1940 to present, Copernicus Climate Change Service (C3S) Climate Data Store (CDS), https://doi.org/10.24381/cds.adbb2d47, last access: 07 February 2024, 2023.

Hönninger, G., von Friedeburg, C., and Platt, U.: Multi axis differential optical absorption spectroscopy (MAX-DOAS), Atmospheric Chemistry and Physics, 4, 231–254, https://doi.org/10.5194/acp-4-231-2004, 2004.

Ingmann, P., Veihelmann, B., Langen, J., Lamarre, D., Stark, H., and Courrèges-Lacoste, G. B.: Requirements for the GMES Atmosphere Service and ESA's implementation concept: Sentinels-4/-5 and -5p, Remote Sensing of Environment, 120, 58–69, https://doi.org/https://doi.org/10.1016/j.rse.2012.01.023, the Sentinel Missions - New Opportunities for Science, 2012.

Kim, J., Jeong, U., Ahn, M.-H., Kim, J. H., Park, R. J., Lee, H., Song, C. H., Choi, Y.-S., Lee, K.-H., Yoo, J.-M., Jeong, M.-J., Park, S. K., Lee, K.-M., Song, C.-K., Kim, S.-W., Kim, Y. J., Kim, S.-W., Kim, M., Go, S., Liu, X., Chance, K., Miller, C. C., Al-Saadi, J., Veihelmann, B., Bhartia, P. K., Torres, O., Abad, G. G., Haffner, D. P., Ko, D. H., Lee, S. H., Woo, J.-H., Chong, H., Park, S. S., Nicks, D., Choi, W. J., Moon, K.-J., Cho, A., Yoon, J., kyun Kim, S., Hong, H., Lee, K., Lee, H., Lee, S., Choi, M., Veefkind, P., Levelt, P. F., Edwards, D. P., Kang, M., Eo, M., Bak, J., Baek, K., Kwon, H.-A., Yang, J., Park, J., Han, K. M., Kim, B.-R., Shin, H.-W., Choi, H., Lee, E., Chong, J., Cha, Y., Koo, J.-H., Irie, H., Hayashida, S., Kasai, Y., Kanaya, Y., Liu, C., Lin, J., Crawford, J. H., Carmichael, G. R., Newchurch, M. J., Lefer, B. L., Herman, J. R., Swap, R. J., Lau, A. K. H., Kurosu, T. P., Jaross, G., Ahlers, B., Dobber, M., McElroy, C. T., and Choi, Y.: New Era of Air Quality Monitoring from Space: Geostationary Environment Monitoring Spectrometer (GEMS), Bulletin of the American Meteorological Society, 101, E1 – E22, https://doi.org/10.1175/BAMS-D-18-0013.1, 2020.

Kim, S., Kim, D., Hong, H., Chang, L.-S., Lee, H., Kim, D.-R., Kim, D., Yu, J.-A., Lee, D., Jeong, U., Song, C.-K., Kim, S.-W., Park, S. S., Kim, J., Hanisco, T. F., Park, J., Choi, W., and Lee, K.: First-time comparison between NO2 vertical columns from Geostationary

Environmental Monitoring Spectrometer (GEMS) and Pandora measurements, Atmospheric Measurement Techniques, 16, 3959–3972, https://doi.org/10.5194/amt-16-3959-2023, 2023.

Lambert, J.-C., Keppens, A., Compernolle, S., Eichmann, K.-U., de Graaf, M., Hubert, D., Langerock, B., Ludewig, A., Sha, M., Verhoelst, T., Wagner, T., Ahn, C., Argyrouli, A., Balis, D., Chan, K., Coldewey-Egbers, M., Smedt, I. D., Eskes, H., Fjæraa, A., Garane, K., Gleason, J., Goutail, F., Granville, J., Hedelt, P., Ahn, C., Heue, K.-P., Jaross, G., Kleipool, Q., Koukouli, M., Lutz, R., Velarte, M. M., Michailidis, K., Nanda, S., Niemeijer, S., Pazmiño, A., Pinardi, G., Richter, A., Rozemeijer, N., Sneep, M., Zweers, D. S., Theys, N., Tilstra, G., Torres, O., Valks, P., van Geffen, J., Vigouroux, C., Wang, P., , and Weber., M.: Quarterly Validation Report of the Copernicus Sentinel-5 Precursor Operational Data Products: April 2018 – November 2023, Tech. rep., last access: 29 February 2024, 2023.

Lange, K., Richter, A., and Burrows, J. P.: Variability of nitrogen oxide emission fluxes and lifetimes estimated from Sentinel-5P TROPOMI observations, Atmospheric Chemistry and Physics, 22, 2745–2767, https://doi.org/10.5194/acp-22-2745-2022, 2022.

Lange, K., Richter, A., Schönhardt, A., Meier, A. C., Bösch, T., Seyler, A., Krause, K., Behrens, L. K., Wittrock, F., Merlaud, A., Tack, F., Fayt, C., Friedrich, M. M., Dimitropoulou, E., Van Roozendael, M., Kumar, V., Donner, S., Dörner, S., Lauster, B., Razi, M., Borger, C., Uhlmannsiek, K., Wagner, T., Ruhtz, T., Eskes, H., Bohn, B., Santana Diaz, D., Abuhassan, N., Schüttemeyer, D., and Burrows, J. P.: Validation of Sentinel-5P TROPOMI tropospheric $NO_2$ products by comparison with $NO_2$ measurements from airborne imaging DOAS, ground-based stationary DOAS, and mobile car DOAS measurements during the S5P-VAL-DE-Ruhr campaign, Atmospheric Measurement Techniques, 16, 1357–1389, https://doi.org/10.5194/amt-16-1357-2023, 2023.

Lee, H., Park, J., and Hong, H.: Geostationary Environment Monitoring Spectrometer (GEMS), Algorithm Theoretical Basis Document, NO2 Retrieval Algorithm, Tech. rep., Environmental Satellite Center, National Institute of Environmental Research, Ministry of Environment, Issue 1.1, available at https://nesc.nier.go.kr/en/html/satellite/doc/doc.do, last access: 23 February 2024, 2020.

Levelt, P. F., van den Oord, G. H., Dobber, M. R., Malkki, A., Visser, H., de Vries, J., Stammes, P., Lundell, J. O., and Saari, H.: The ozone monitoring instrument, IEEE Transactions on geoscience and remote sensing, 44, 1093–1101, https://doi.org/10.1109/TGRS.2006.872333, 2006.

Lorente, A., Boersma, K., Eskes, H., Veefkind, J., Van Geffen, J., de Zeeuw, M., van der Gon, H. D., Beirle, S., and Krol, M.: Quantification of nitrogen oxides emissions from build-up of pollution over Paris with TROPOMI, Scientific reports, 9, 1–10, https://doi.org/10.1038/s41598-019-56428-5, 2019.

Ma, J. Z., Beirle, S., Jin, J. L., Shaiganfar, R., Yan, P., and Wagner, T.: Tropospheric $NO_2$ vertical column densities over Beijing: results of the first three years of ground-based MAX-DOAS measurements (2008–2011) and satellite validation, Atmospheric Chemistry and Physics, 13, 1547–1567, https://doi.org/10.5194/acp-13-1547-2013, 2013.

Munro, R., Eisinger, M., Anderson, C., Callies, J., Corpaccioli, E., Lang, R., Lefebvre, A., Livschitz, Y., and Albinana, A. P.: GOME-2 on MetOp, in: Proc. of The 2006 EUMETSAT Meteorological Satellite Conference, Helsinki, Finland, vol. 1216, p. 48, 2006.

Oak, Y. J., Jacob, D. J., Balasus, N., Yang, L. H., Chong, H., Park, J., Lee, H., Lee, G. T., Ha, E. S., Park, R. J., Kwon, H.-A., and Kim, J.: A bias-corrected GEMS geostationary satellite product for nitrogen dioxide using machine learning to enforce consistency with the TROPOMI satellite instrument, EGUsphere, 2024, 1–19, https://doi.org/10.5194/egusphere-2024-393, 2024.

Pandonia Global Network: PGN data archive [data set], http://data.pandonia-global-network.org/, last access: 4 February 2023.

Penn, E. and Holloway, T.: Evaluating current satellite capability to observe diurnal change in nitrogen oxides in preparation for geostationary satellite missions, Environmental Research Letters, 15, 034 038, https://doi.org/10.1088/1748-9326/ab6b36, 2020.

Pinardi, G., Van Roozendael, M., Hendrick, F., Theys, N., Abuhassan, N., Bais, A., Boersma, F., Cede, A., Chong, J., Donner, S., Drosoglou, T., Dzhola, A., Eskes, H., Frieß, U., Granville, J., Herman, J. R., Holla, R., Hovila, J., Irie, H., Kanaya, Y., Karagkiozidis, D., Kouremeti,

N., Lambert, J.-C., Ma, J., Peters, E., Piters, A., Postylyakov, O., Richter, A., Remmers, J., Takashima, H., Tiefengraber, M., Valks, P., Vlemmix, T., Wagner, T., and Wittrock, F.: Validation of tropospheric $NO_2$ column measurements of GOME-2A and OMI using MAX-DOAS and direct sun network observations, Atmospheric Measurement Techniques, 13, 6141–6174, https://doi.org/10.5194/amt-13-6141-2020, 2020.

Platt, U. and Perner, D.: Direct measurements of atmospheric CH2O, HNO2, O3, NO2, and SO2 by differential optical absorption in the near UV, Journal of Geophysical Research: Oceans, 85, 7453–7458, https://doi.org/10.1029/JC085iC12p07453, 1980.

Rozanov, V., Rozanov, A., Kokhanovsky, A., and Burrows, J.: Radiative transfer through terrestrial atmosphere and ocean: Software package SCIATRAN, Journal of Quantitative Spectroscopy and Radiative Transfer, 133, 13–71, https://doi.org/10.1016/j.jqsrt.2013.07.004, 2014.

Seinfeld, J. H. and Pandis, S. N.: Atmospheric Chemistry and Physics, John Wiley & Sons Inc., Hoboken, New Jersey, 2006.

Sentinel-5P Pre-Operations Data Hub: Offline L2 $NO_2$ [data set], https://s5phub.copernicus.eu/, last access: 21 February 2022.

Seo, S., Kim, S.-W., Kim, K.-M., Richter, A., Lange, K., Burrows, J. P., Park, J., Hong, H., Lee, H., Jeong, U., and Kim, J.: Diurnal variations of $NO_2$ tropospheric vertical column density over the Seoul Metropolitan Area from the Geostationary Environment Monitoring Spectrometer (GEMS): seasonal differences and impacts of varying *a priori* $NO_2$ profile data, Atmospheric Measurement Techniques Discussions, 2024, 1–28, https://doi.org/10.5194/amt-2024-33, 2024.

Souri, A. H., Kumar, R., Chong, H., Golbazi, M., Knowland, K. E., Geddes, J., and Johnson, M. S.: Decoupling in the vertical shape of HCHO during a sea breeze event: The effect on trace gas satellite retrievals and column-to-surface translation, Atmospheric Environment, 309, 119 929, https://doi.org/https://doi.org/10.1016/j.atmosenv.2023.119929, 2023.

Spurr, R. J.: VLIDORT: A linearized pseudo-spherical vector discrete ordinate radiative transfer code for forward model and retrieval studies in multilayer multiple scattering media, Journal of Quantitative Spectroscopy and Radiative Transfer, 102, 316–342, https://doi.org/10.1016/j.jqsrt.2006.05.005, 2006.

Stavrakou, T., Müller, J.-F., Bauwens, M., Boersma, K., and van Geffen, J.: Satellite evidence for changes in the NO2 weekly cycle over large cities, Scientific reports, 10, 1–9, https://doi.org/10.1038/s41598-020-66891-0, 2020.

Tilstra, L. G., de Graaf, M., Trees, V., Litvinov, P., Dubovik, O., and Stammes, P.: A directional surface reflectance climatology determined from TROPOMI observations, Atmospheric Measurement Techniques Discussions, 2023, 1–29, https://doi.org/10.5194/amt-2023-222, 2023.

van der A, R. J., Eskes, H. J., Boersma, K. F., van Noije, T. P. C., Van Roozendael, M., De Smedt, I., Peters, D. H. M. U., and Meijer, E. W.: Trends, seasonal variability and dominant NOx source derived from a ten year record of NO2 measured from space, Journal of Geophysical Research: Atmospheres, 113, D04 302, https://doi.org/10.1029/2007JD009021, 2008.

van Geffen, J., Eskes, H., Boersma, K., and Veefkind, J.: TROPOMI ATBD of thetotal and tropospheric $NO_2$ data products, Tech. rep., 5P-KNMI-L2-0005-RP, Issue 2.4.0, available at https://sentinel.esa.int/documents/247904/2476257/sentinel-5p-tropomi-atbd-no2-data-products, last access: 18 December 2022, 2022.

Veefkind, J., Aben, I., McMullan, K., Förster, H., de Vries, J., Otter, G., Claas, J., Eskes, H., de Haan, J., Kleipool, Q., van Weele, M., Hasekamp, O., Hoogeveen, R., Landgraf, J., Snel, R., Tol, P., Ingmann, P., Voors, R., Kruizinga, B., Vink, R., Visser, H., and Levelt, P.: TROPOMI on the ESA Sentinel-5 Precursor: A GMES mission for global observations of the atmospheric composition for climate, air quality and ozone layer applications, Remote Sensing of Environment, 120, 70–83, https://doi.org/10.1016/j.rse.2011.09.027, the Sentinel Missions - New Opportunities for Science, 2012.

Verhoelst, T., Compernolle, S., Pinardi, G., Lambert, J.-C., Eskes, H. J., Eichmann, K.-U., Fjæraa, A. M., Granville, J., Niemeijer, S., Cede, A., Tiefengraber, M., Hendrick, F., Pazmiño, A., Bais, A., Bazureau, A., Boersma, K. F., Bognar, K., Dehn, A., Donner, S., Elokhov,

A., Gebetsberger, M., Goutail, F., Grutter de la Mora, M., Gruzdev, A., Gratsea, M., Hansen, G. H., Irie, H., Jepsen, N., Kanaya, Y., Karagkiozidis, D., Kivi, R., Kreher, K., Levelt, P. F., Liu, C., Müller, M., Navarro Comas, M., Piters, A. J. M., Pommereau, J.-P., Portafaix, T., Prados-Roman, C., Puentedura, O., Querel, R., Remmers, J., Richter, A., Rimmer, J., Rivera Cárdenas, C., Saavedra de Miguel, L., Sinyakov, V. P., Stremme, W., Strong, K., Van Roozendael, M., Veefkind, J. P., Wagner, T., Wittrock, F., Yela González, M., and Zehner, C.: Ground-based validation of the Copernicus Sentinel-5P TROPOMI $NO_2$ measurements with the NDACC ZSL-DOAS, MAX-DOAS and Pandonia global networks, Atmospheric Measurement Techniques, 14, 481–510, https://doi.org/10.5194/amt-14-481-2021, 2021.

Wagner, T., Ibrahim, O., Shaiganfar, R., and Platt, U.: Mobile MAX-DOAS observations of tropospheric trace gases, Atmospheric Measurement Techniques, 3, 129–140, https://doi.org/10.5194/amt-3-129-2010, 2010.

Wallace, J. M. and Hobbs, P. V.: Atmospheric science: an introductory survey, vol. 92, Elsevier, https://www.ebook.de/de/product/4444872/john_m_university_of_washington_seattle_u_s_a_wallace_peter_v_university_of_washington_seattle_u_s_a_hobbs_atmospheric_science.html, 2006.

Williams, J. E., Boersma, K. F., Le Sager, P., and Verstraeten, W. W.: The high-resolution version of TM5-MP for optimized satellite retrievals: description and validation, Geoscientific Model Development, 10, 721–750, https://doi.org/10.5194/gmd-10-721-2017, 2017.

Wittrock, F., Oetjen, H., Richter, A., Fietkau, S., Medeke, T., Rozanov, A., and Burrows, J. P.: MAX-DOAS measurements of atmospheric trace gases in Ny-Ålesund - Radiative transfer studies and their application, Atmospheric Chemistry and Physics, 4, 955–966, https://doi.org/10.5194/acp-4-955-2004, 2004.

Xu, T., Zhang, C., Xue, J., Hu, Q., Xing, C., and Liu, C.: Estimating Hourly Nitrogen Oxide Emissions over East Asia from Geostationary Satellite Measurements, Environmental Science & Technology Letters, https://doi.org/10.1021/acs.estlett.3c00467, 2023.

Yang, L. H., Jacob, D. J., Colombi, N. K., Zhai, S., Bates, K. H., Shah, V., Beaudry, E., Yantosca, R. M., Lin, H., Brewer, J. F., Chong, H., Travis, K. R., Crawford, J. H., Lamsal, L. N., Koo, J.-H., and Kim, J.: Tropospheric $NO_2$ vertical profiles over South Korea and their relation to oxidant chemistry: implications for geostationary satellite retrievals and the observation of $NO_2$ diurnal variation from space, Atmospheric Chemistry and Physics, 23, 2465–2481, https://doi.org/10.5194/acp-23-2465-2023, 2023a.

Yang, L. H., Jacob, D. J., Dang, R., Oak, Y. J., Lin, H., Kim, J., Zhai, S., Colombi, N. K., Pendergrass, D. C., Beaudry, E., Shah, V., Feng, X., Yantosca, R. M., Chong, H., Park, J., Lee, H., Lee, W.-J., Kim, S., Kim, E., Travis, K. R., Crawford, J. H., and Liao, H.: Interpreting Geostationary Environment Monitoring Spectrometer (GEMS) geostationary satellite observations of the diurnal variation in nitrogen dioxide ($NO_2$) over East Asia, Atmospheric Chemistry and Physics, 24, 7027–7039, https://doi.org/10.5194/acp-24-7027-2024, 2024.

Yang, Q., Kim, J., Cho, Y., Lee, W.-J., Lee, D.-W., Yuan, Q., Wang, F., Zhou, C., Zhang, X., Xiao, X., Guo, M., Guo, Y., Carmichael, G. R., and Gao, M.: A synchronized estimation of hourly surface concentrations of six criteria air pollutants with GEMS data, npj Climate and Atmospheric Science, 6, https://doi.org/10.1038/s41612-023-00407-1, 2023b.

Zhang, Y., Lin, J., Kim, J., Lee, H., Park, J., Hong, H., Van Roozendael, M., Hendrick, F., Wang, T., Wang, P., He, Q., Qin, K., Choi, Y., Kanaya, Y., Xu, J., Xie, P., Tian, X., Zhang, S., Wang, S., Cheng, S., Cheng, X., Ma, J., Wagner, T., Spurr, R., Chen, L., Kong, H., and Liu, M.: A research product for tropospheric NO2 columns from Geostationary Environment Monitoring Spectrometer based on Peking University OMI NO2 algorithm, Atmospheric Measurement Techniques, 16, 4643–4665, https://doi.org/10.5194/amt-16-4643-2023, 2023.

Zoogman, P., Liu, X., Suleiman, R., Pennington, W., Flittner, D., Al-Saadi, J., Hilton, B., Nicks, D., Newchurch, M., Carr, J., Janz, S., Andraschko, M., Arola, A., Baker, B., Canova, B., Chan Miller, C., Cohen, R., Davis, J., Dussault, M., Edwards, D., Fishman, J., Ghulam, A., González Abad, G., Grutter, M., Herman, J., Houck, J., Jacob, D., Joiner, J., Kerridge, B., Kim, J., Krotkov, N., Lamsal, L., Li, C., Lindfors, A., Martin, R., McElroy, C., McLinden, C., Natraj, V., Neil, D., Nowlan, C., O'Sullivan, E., Palmer, P., Pierce, R.,

Pippin, M., Saiz-Lopez, A., Spurr, R., Szykman, J., Torres, O., Veefkind, J., Veihelmann, B., Wang, H., Wang, J., and Chance, K.: Tropospheric emissions: Monitoring of pollution (TEMPO), Journal of Quantitative Spectroscopy and Radiative Transfer, 186, 17–39, https://doi.org/https://doi.org/10.1016/j.jqsrt.2016.05.008, satellite Remote Sensing and Spectroscopy: Joint ACE-Odin Meeting, October 2015, 2017.